



Online prediction of the hand configuration using ultrasound images of the forearm

David Sierra González



MASTER THESIS**ONLINE PREDICTION OF THE HAND
CONFIGURATION USING ULTRASOUND
IMAGES OF THE FOREARM**

Author:

David Sierra González, BSc

Supervisor:

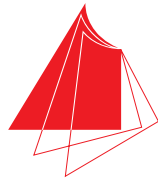
Dr. Claudio Castellini

The Institute's head

Prof. Dr. G. Hirzinger

This document comprises 95 pages, 43 figures and 14 tables

*Master in Mechatronic and Micro-Mechatronic Systems
Hochschule Karlsruhe - Technik und Wirtschaft*



**Hochschule Karlsruhe
Technik und Wirtschaft**
UNIVERSITY OF APPLIED SCIENCES

MASTER THESIS

**ONLINE PREDICTION OF THE HAND CONFIGURATION
USING ULTRASOUND IMAGES OF THE FOREARM**

Project developed by

David Sierra González

with the supervision of

**Dr. Claudio Castellini
Prof. Dr. Astrid Laubenheimer
Prof. Dr. Michael C. Wilhelm**

at the Deutsches Zentrum für Luft- und Raumfahrt e.V.

August 2012



*Máster en Ingeniería Mecatrónica
Escuela Politécnica de Ingeniería de Gijón
Universidad de Oviedo*



TESIS DE MÁSTER

**PREDICCIÓN ONLINE DE LA CONFIGURACIÓN DE LA
MANO MEDIANTE IMÁGENES DE ULTRASONIDOS DEL
ANTEBRAZO**

Proyecto desarrollado por

David Sierra González

con la supervisión de

Dr. Claudio Castellini

Prof. Dr. Astrid Laubenheimer

Prof. Dr. Michael C. Wilhelm

en el Deutsches Zentrum für Luft- und Raumfahrt e.V.

Agosto de 2012





Master-Thesis

David Sierra González

Arbeitsplatz

Hochschule Karlsruhe – Technik und Wirtschaft
Fakultät für Maschinenbau und Mechatronik
76133 Karlsruhe

DLR – Deutsches Zentrum für Luft- und Raumfahrt e.V.
Institut für Robotik und Mechatronik
Standort Oberpfaffenhofen, 82234 Weßling

Betreuer am Arbeitsplatz

Dr. Claudio Castellini
Institute of Robotics and Mechatronics
DLR Oberpfaffenhofen

Betreuender Dozent

Prof. Dr.-Ing. Astrid Laubenheimer
Fakultät für Informatik und Wirtschaftsinformatik

Datum der Ausgabe

1.4.2012

Abgabetermin

31.8.2012

Kurzthema:

***Online-Schätzung der Handkonfiguration aus
Ultraschallbilder***

Aufgabenstellung

Das Ziel ist die Rekonstruktion der Fingerpositionen mittels Ultraschallbildern des Unterarmes. Das vorhandene System soll verbessert und optimiert werden. Am Ende soll ein Online System zur Verfügung stehen.

Im Einzelnen sind die folgenden Punkte zu bearbeiten:

- Komplettes Redesign des Systems und Portierung nach C#, dabei soll die Synchronisation der Daten, die mit Framegrabber und Cyberglove erhalten werden, verbessert werden.
- Vergleiche die Auswirkungen der unterschiedlichen Sondenhalterungen auf die Leistung des Systems, untersuche außerdem in wie weit die Stabilität des System über die Zeit mit *Optical Flow* verbessert werden kann.
- Erreiche ein stabiles System, das ohne Verschlechterung der Leistung über eine längere Zeit, z.B. 30 Minuten, funktioniert.
- Untersuche die Einführung eines Online Learning Systems: Ridge Regression
- Teste das System an mehreren Versuchsobjekten
- Dokumentation und Präsentation der Ergebnisse

**Vorsitzender des
Prüfungsausschusses**

Prof. Dipl.-Wirtsch.-Ing.
Fritz J. Neff

**Betreuender Dozent an der
HSKA**

Prof. Dr.-Ing. Astrid
Laubenheimer

**Betreuender Dozent am
Arbeitsplatz/extern**

Dr. Claudio Castellini

Declaration

I certify that this thesis is entirely my own work. Where any external source of information has been used, it has been acknowledged. This work has not been submitted, either in whole or in part, for a degree at this or any other university.

Place

Date

David Sierra González

Acknowledgments

In the first place I would like to thank Dr. Claudio Castellini for the fantastic opportunity of joining the DLR's Institute of Robotics and Mechatronics and his continuous support and encouragement. I extend my gratitude to Dr. Patrick van der Smagt and the whole Bionics Group. From the Hochschule Karlsruhe I have to thank Prof. Dr. Ing. Astrid Laubenheimer for her guidance and the interest she has shown in my work and Prof. Dipl.-Wirtsch.-Ing. Fritz J. Neff and Annette Knödler for their invaluable support. Back in Spain, professors Dr. Miguel Ángel José Prieto, Dr. Juan Carlos Álvarez Álvarez and Dr. José Manuel Sierra Velasco encouraged me to leave my shell and finish my studies abroad. I will never be grateful enough for that. Finally, I cannot forget all those that have been at my side during my student years. I would have never come this far without the unconditional support of my mother Dulce and all my friends at the University of Oviedo and at the Hochschule Karlsruhe.

Abstract

Phantom pain is a problem that affects a certain number of persons who have lost a hand. The amputees affected by phantom pain feel as if the fingers they no longer have were clutching. They are incapable of alter this in any way which translates in discomfort and even pain.

Several treatments for this pain are based in the idea that if the patient can see his fingers moving he will no longer feel them clutching, thus eradicating any discomfort or pain. This is called visual feedback and the project developed in this thesis also works based on this concept.

Previous studies have demonstrated a linear relationship between first degree features extracted from ultrasound images taken from the forearm and the angles at which the fingers of the hand are. Using this information it is possible to train a system that in real time predicts the position of the fingers while receiving a feed of ultrasound images of the forearm.

With the target of reaching a robust system capable of running without decay in the performance overtime several approaches were taken. A more dynamic training system was implemented using incremental linear regression. This allows the patient to switch back and forth from the training part of the experiment to the prediction phase. While predicting, a 3D hand model that moves based exclusively on the information extracted from the ultrasound images is displayed on the screen. With this training method, if the prediction is not satisfactory, it is possible to go back to training and 'fine tune' specific finger movements.

A physical setup that keeps the transducer of the ultrasound system fixed to the arm was developed. However, it does not keep the patients from turning their wrists while performing the different finger movements. This tiny pronation of the wrist produces radical changes in the ultrasound images and ultimately in the quality of the prediction. An idea of how to tackle this problem based on a magnetic tracker attached to the wrist is presented.

Kurzfassung

Viele Personen die ein Körperteil wie die Hand verloren haben, werden von Phantomschmerzen geplagt. Dabei fühlen diese Betroffenen, dass ihre fehlenden Finger sich in einem dauerhaften, angespannten Zustand befinden. Es ist Ihnen nicht möglich diesen Zustand zu ändern, wodurch ein deutliches Gefühl der Unannehmlichkeit und sogar Schmerz hervorgerufen wird.

Einige Behandlungsmethoden für diese Art von Phantomschmerzen basieren auf der Idee, dass dem Patienten die Bewegung seiner fehlenden Finger nachgebildet und ihm gezeigt wird, wodurch das Spannungsgefühl und die damit verbundenen Schmerzen verschwinden. Dieses Prinzip nennt sich optisches Feedback. Das Ergebnis der vorliegenden Arbeit ist die Basis eines weiterführenden Projekts im Deutschen Zentrum für Luft- und Raumfahrt, das mit diesem Konzept arbeitet und mit Hilfe von Patienten validiert wird.

Durch frühere Studien wird gezeigt, dass ein linearer Zusammenhang zwischen der Darstellung der Unterarmmuskulatur mit Hilfe eines Ultraschallgeräts, also dem aktuellen Aktivierungszustand der Muskeln, und den entsprechenden Gelenkwinkeln der Finger besteht. Mit Hilfe dieser Information war es möglich ein System zu erstellen, das mit Hilfe von Ultraschalldaten und nach Anpassung auf den jeweiligen Probanden in der Trainingsphase die Fingerpositionen in Echtzeit vorhersagen und anzeigen kann.

Es wurden zahlreiche Ansätze ausgearbeitet um ein robustes System zu erzeugen, welches dauerhaft und ohne Verlust an Genauigkeit Ergebnisse liefert. Die Fähigkeit des Systems, sich während der Trainingsphase auf das jeweilige Subjekt anzupassen, konnte durch die Verwendung einer inkrementellen, linearen Regression verbessert werden. Dadurch ist es möglich, bei Bedarf zwischen dem eigentlichen Ablauf des Programms und der Trainingsphase zu wechseln, wodurch einzelne Bewegungen der Ultraschallaufnahmen wiederholt und somit eine Feinabstimmung einzelner Finger erfolgen kann. Die Qualität der Behandlung kann dadurch deutlich gesteigert werden. Zur Anschauung kann dem Patienten während der Vorhersage ein bewegliches 3D Model seiner Hand dargestellt werden, welches ausschließlich durch Ultraschalldaten der Unterarmmuskulatur erzeugt wird.

Neben diesen softwaretechnischen Neuerungen wurde die Halterung der Ultraschallsonde, die am menschlichen Arm befestigt wird, weiterentwickelt. Denn das Problem bei der

Befestigung der Sonde ist, dass selbst kleine Rotationen des Unterarms und die damit verbundene Verschiebung des Ultraschall-Messgebers auf der Haut zu drastischen Änderungen in den Aufnahmen und damit zu einem deutlichen Verlust der Aufnahmequalität führt. Zusätzlich zur mechanischen Vorrichtung sorgt ein magnetischer Positions- und Winkelgeber am Unterarm dafür, dass der Einfluss dieser Rotation durch die Software erfasst und dadurch rechnerisch verringert wird.

Resumen

El dolor fantasma es un problema que afecta a gran parte de las personas que han perdido una mano. Los amputados afectados por dolor fantasma sienten como si los dedos de la mano que han perdido estuvieran fuertemente apretados. Al ser incapaces de alterar esta situación sufren de un constante malestar y en ocasiones incluso sienten dolor.

Varios tratamientos para el dolor fantasma se basan en la idea de que si el paciente pudiera ver sus dedos moviéndose la sensación de tenerlos apretados desaparecería, eliminando así cualquier malestar o dolor. Este concepto se conoce como retroalimentación visual y en él está basado el trabajo desarrollado en esta tesis.

Estudios han demostrado que existe una relación lineal entre las imágenes de ultrasonidos tomadas en el antebrazo y los ángulos en que se encuentran los dedos de la mano. Usando esta información es posible desarrollar un sistema que prediga en tiempo real la posición de los dedos de la mano computando únicamente imágenes de ultrasonidos tomadas en el antebrazo.

Con el objetivo de obtener un sistema robusto se siguieron diversas líneas de trabajo. El sistema se implementó usando una regresión lineal incremental, lo que permite que el paciente pueda cambiar en cualquier momento de la parte de entrenamiento del experimento a la parte de predicción y viceversa. Cuando se está prediciendo, un modelo 3D de una mano se muestra en pantalla. Este modelo se mueve basado exclusivamente en la información extraída de las imágenes de ultrasonidos del antebrazo del paciente. Con el sistema de entrenamiento descrito, si la calidad de la predicción no es la deseada, siempre es posible volver a la fase de entrenamiento y añadir más información hasta que el rendimiento sea el deseado.

Adicionalmente se implementó una estructura física que mantiene la sonda de ultrasonidos completamente fijada al brazo durante el experimento. Sin embargo, esta estructura no puede evitar que los pacientes giren la muñeca al realizar los diferentes movimientos de los dedos de la mano. Esta minúscula e involuntaria pronación se traduce en cambios drásticos en las características de las imágenes de ultrasonidos y, por consiguiente, en la calidad de la predicción. Con el objetivo de atajar este problema se presenta una idea basada en un sensor magnético fijado a la muñeca.

Contents

1	Introduction	1
1.1	Motivation	1
1.2	Overview	3
2	State of the art	5
3	Problem analysis	9
3.1	Problem description	9
3.2	General approach	10
3.3	Previous work	11
3.4	Goals	12
4	Theoretical framework	15
4.1	Ultrasonography	15
4.1.1	Sound and wave theory	15
4.1.1.1	Acoustic Variables	16
4.1.1.2	Parameters of sound	17
4.1.2	Ultrasound production	19
4.1.3	Transducers	20
4.1.3.1	Mechanical Transducers	20
4.1.3.2	Electronic Transducers	21
4.1.4	Display modes	22
4.1.4.1	A-Mode	22
4.1.4.2	B-Mode	23
4.1.4.3	M-Mode	24
4.1.5	Ultrasound-tissue interaction	24
4.2	Hand and forearm anatomy	26
4.2.1	Terminology	26
4.2.2	Forearm	27
4.2.2.1	Forearm muscles that move the fingers	28
4.2.3	Hand	37

4.2.3.1	Bones	37
4.2.3.2	Joints	37
4.2.4	Phantom limb pain	38
4.3	Machine Learning	40
4.3.1	Regression Analysis	40
4.4	Image processing	43
4.4.1	Digital image	43
4.4.1.1	Image definition	44
4.4.1.2	Number of planes	44
4.4.1.3	Conversion from color to grayscale	44
4.4.2	First order surfaces	45
4.4.3	Optical flow	45
4.5	Analysis of results	45
4.5.1	Mean	46
4.5.2	Standard deviation	46
4.5.3	Mean Absolute Error	46
4.5.4	Normalized Root Mean Squared Error	46
4.5.5	Correlation Coefficient	47
5	Hardware	49
5.1	Ultrasound portable system	49
5.2	Cyberglove	51
5.3	Framegrabber	52
5.4	Flock of birds	53
5.5	Probe holder	54
6	Software	57
6.1	Visual Studio C#	57
6.2	MVTec's Halcon	58
6.2.1	Optical flow in Halcon	58
6.3	MATLAB	59
6.4	Numerical library: ALGLIB	59
6.5	Hand Model	60
7	System analysis	61
7.1	Modes of operation	61
7.1.1	Method: Cyberglove	62
7.1.2	Method: Stimulus	62
7.2	Graphical User Interface	63
7.3	Inside the C# application	65
7.3.1	Interactions between threads and timing analysis	67

7.4 Compensation of the pronation wrist	69
8 Experiments	75
8.1 Preliminary experiment	75
8.1.1 Description	75
8.1.2 Results	76
8.1.3 Analysis of results	77
8.2 Main experiment	78
8.2.1 Description	78
8.2.2 Results	80
8.2.2.1 Using Cyberglove	80
8.2.2.2 Using stimulus	81
8.2.3 Analysis of results	82
9 Conclusions and future work	87
References	93

List of Figures

1.1	Mirror box therapy	2
1.2	Patient during an experiment	3
2.1	i-limb ultra prosthetic hand	7
3.1	Finger movements to be predicted	10
3.2	Basic approach to the solution	11
4.1	Production of sound by variations in air pressure	16
4.2	Wires of a US transducer	21
4.3	Linear sequenced array available at the DLR	22
4.4	Ultrasound imaging modes	23
4.5	B-mode image of the upper abdomen	24
4.6	Different types of ultrasound wave-tissue interactions	25
4.7	Overview of bones and joints of the upper limb	31
4.8	Muscles of the flexor aspect of the upper limb	32
4.9	Muscles of the extensor aspect of the upper limb	33
4.10	Cross-sectional view of the right mid-forearm	35
4.11	Transverse section US imaging of the mid-forearm	35
4.12	Transverse section through the lower third of the forearm	36
4.13	Transverse section US imaging of the distal anterior forearm	36
4.14	Hand joint movements	39
5.1	General scheme of the setup	51
5.2	Ultrasound system LOGIQ e	52
5.3	Cyberglove	53
5.4	VGA Framegrabber	53
5.5	Flock of birds	54
5.6	PRO/Engineering model of the probe holder	55
5.7	Arm adjustable probe holder	55
5.8	Evolution of the probe holder	56

7.1	GUI during an experiment	63
7.2	Natural flow of an experiment	66
7.3	Data rates from the Cyberglove and the Flock of Birds	67
7.4	Data rate from the framegrabber	67
7.5	Example of teared frame	70
7.6	Data rate from the framegrabber without teared frames	70
7.7	Changes in the US images with the wrist angle	71
7.8	Shifting of the regions of interest proportionally to the wrist angle	72
7.9	Effect of the dynamic grid on the error	73
8.1	Testing of physical setups	77
8.2	Test subject during the experiment	79
8.3	Comparison of NRMSE before and after retraining with Cyberglove	81
8.4	Comparison of CC before and after retraining with Cyberglove	81
8.5	Comparison of NRMSE before and after retraining with stimulus	83
8.6	Comparison of CC before and after retraining with stimulus	83
8.7	Evolution of the prediction of the index finger for subject #1	84

List of Tables

4.1	Media and their propagation speeds	17
4.2	Acoustic impedances of different body tissues and organs	19
4.3	Anatomic terminology relative to directions	26
4.4	Anatomic terminology relative to movements	27
4.5	Forearm muscles that move the wrist joint, hand and fingers	34
5.1	Optimized parameters for the ultrasound system	50
5.2	Characteristics of the Flock of Birds	54
7.1	Modes of operation	61
8.1	Evolution of the NRMSE of the two setups during the experiment	78
8.2	Conditions of the main experiment	78
8.3	Prediction results with Cyberglove before retraining	80
8.4	Prediction results with Cyberglove after retraining	80
8.5	Prediction results with stimulus before retraining	82
8.6	Prediction results with stimulus after retraining	82

List of Acronyms

AHP	Active Hand Prosthesis.
CC	Correlation Coefficient.
CMC	Carpometacarpal.
DIP	Distal Interphalangeal.
DLR	Deutsches Zentrum für Luft- und Raumfahrt.
DoF	Degree Of Freedom.
EEG	Electroencephalography.
EMG	Electromyography.
GUI	Graphical User Interface.
IP	Interphalangeal.
MAE	Mean Absolute Error.
MCP	Metacarpophalangeal.
NRMSE	Normalized Root Mean Square Error.
PIP	Proximal Interphalangeal.
S/N	Signal-to-noise ratio.
US	Ultrasound.

1

Introduction

1.1 Motivation

Phantom pain sensations are described as perceptions that an individual experiences relating to a limb or an organ that is not physically part of the body. Many patients experience pain as a result of a clenched phantom limb and because phantom limbs are not under voluntary control unclenching becomes impossible. One of the traditional treatments for phantom limb pain in amputees is the *mirror box therapy*. In this treatment the patient places the good limb outside a box facing a mirror and the stump inside. The patient looks then in the mirror and tries to perform symmetric movements with both hands. After some time the patient starts feeling as if he were actually moving the lost limb. This happens because the visual feedback that mirror therapy provides replaces the sensory feedback that the brain expects from the missing limb. An usual setup for this therapy can be seen in figure [1.1](#). Through the use of this artificial visual feedback it becomes possible for the patient to “move” the phantom limb and to unclench it from potentially painful positions.

The aim of this project is to achieve the 21st century version of the mirror box therapy. Ultrasound (US) images of the forearm are captured with a portable ultrasound machine and fed into the system. The images are then processed to produce a real-time prediction of the position of the fingers, which is displayed as a 3D hand model on the screen.



Figure 1.1: Mirror box therapy [1]

With this non-invasive system below-elbow amputees and neuropathic pain patients will be able to use the system to ease their phantom limb pain or regain their lost hand function. Another possible application is the control of robotic or prosthetic hands.

This project has been carried out at the Institute of Robotics and Mechatronics of the Deutsches Zentrum für Luft- und Raumfahrt (DLR) in Oberpfaffenhofen, Germany. More specifically the project is managed by the Bionics Group of this institute, which deals with topics such as biomechanics and body-machine interfaces. The Bionics Group is engaged in achieving advancements in the fields of rehabilitation and prosthetics.

The origins of this project can be traced back to 2011, when a paper titled *Ultrasound image features of the wrist are linearly related to finger positions* was written by Dr. Claudio Castellini and Dr. Georg Passig [2]. Ultrasounds were since a long time successfully used as a diagnostic tool for hand musculoskeletal disorders (e.g. rheumatoid arthritis [3]) so it was likely that US images contained enough information to reconstruct -at least partly- the position, velocity and/or force exerted by the fingers. This idea is easily demonstrated by observing US images of the forearm (placing the probe of the US machine, for example, on the ventral side) while performing different movements with the fingers. The correspondence between finger movements and deformation of the images is clear.

Whether or not an amputee will be able to use this system depends principally on the remaining musculoskeletal activity. The movements of muscles and tendons have to be distinguishable when moving the different fingers. In late 2011 an amputee visited the DLR's installations in Oberpfaffenhofen. The 43 years old patient with a remaining limb of 30 cm was asked to mimic the movements of a 3D hand model that was being displayed on a monitor. Figure 1.2 shows the patient during the experiment with the probe of the US machine placed on the lower part of the forearm. The US images taken proved to be

clearly different when asked to move the different fingers. The feasibility of the project was then confirmed.



Figure 1.2: Patient during an experiment (DLR Oberpfaffenhofen, 2011)

1.2 Overview

This document pretends to give a general idea of the work carried out during this Master Thesis. A fair number of technical equipment has been integrated into a single application in order to transform ideas and theory into action.

Even when a lot of code has been written the idea behind this document is to provide a high level view of the solution rather than explaining in detail how every task was programmed. Naturally, there is a special focus on the tests performed as well as in the results obtained, with the final goal of providing an estimation of how valuable the developed system is.

The layout of this thesis and the contents of each chapter are introduced below.

After the motivations discussed in this introductory chapter, different approaches existent to solve this and similar problems are commented in the chapter [State of the art](#).

The chapter [Problem analysis](#) contains a more detailed description of the problem at hand as well as a general explanation of the approach taken. At this point it is already possible to discuss the main differences between this thesis and the previous version of the project and set the goals to be achieved.

The chapter [Theoretical framework](#) includes all the necessary information to understand the problem and the solution implemented. Naturally, references to expand on this information are provided.

A short description of the devices used in this project can be found in the chapter [Hardware](#). The same can be said of the different [Software](#) that has been employed in the development of this thesis.

A simple but thorough study of the working principles of the system can be consulted in the chapter [System analysis](#). At the end of this chapter a theoretical new idea is proposed.

The probably juiciest part of this document comes at the end with the chapter [Experiments](#), which is complemented with the [Conclusions and future work](#).

2

State of the art

Finger motion recognition is a problem that has been addressed in a large number of studies, mostly driven by the need of finding an interface between amputees and Active Hand Prostheses (AHP). With the recent advances in mechatronics it is now possible to build prosthetic hands with multiple active degrees of freedom.

Passive prosthetics are realistic in appearance and semi-functional. These prosthetics are practical when an amputee is most concerned about his image, the weight of the prosthetic and having some minor degree of functionality. On the other hand active prostheses enable the user to grasp and maneuver objects. These prostheses are designed to help increase function and independence. Sensorial feedback completes the picture, making the prosthesis a sensible replacement of the lost hand.

Some of the most advanced commercially available AHPs at the time of writing include the *SensorHand Speed* from *Ottobock* [4] and the *i-limb ultra* from *Touch Bionics* [5]. The *SensorHand* provides a simple claw system, with only one degree of freedom (DOF). The *i-limb* has five, individually powered, articulating fingers as well as a manually rotatable thumb to create different grasping options. They offer a range of 13 automatic hand features (index point, lateral grip, natural hand position, two thumb parking modes, four precision pinch options, four tripod options) and a detection system to tell each individual digit when it has exerted enough pressure to grip an object (and thus stop powering to prevent crushing). However there is no real fine control over single fingers nor a possibility

to control the actuated force.

Within the AHPs it is possible to differentiate two kinds of interfaces between the user and the prosthesis: invasive and non-invasive. Invasive interfaces gather information directly from the user's nervous system, either with brain implants or surgical-implanted electrodes. On the other hand, non-invasive interfaces are easier to use and present a lower cost but because of their lower signal-to-noise ratio (S/N) they require higher signal conditioning.

Focusing on the non-invasive techniques, the most extended approach has been the application of Surface Electromyography (SEMG), which measures the muscle electrical activity that occurs during muscle contraction and relaxation cycles [6]. Muscle activation potentials are gathered by electrodes placed on the patient's forearm skin. These potentials can be used to track which muscles the patient is willing to activate, and with what force. Some problems of this technique are addressed in [7]. The difficulties to produce precision grasp of small objects using SEMG are caused by:

- The SEMG signals detected from the skin surface are the superposition of multiple muscle potentials.
- The electric potentials of the activated muscles, especially those deep layered muscles, such as *extensor indicis*, are affected (attenuated and modulated) by various nonlinear elements, such as fat and tissue, before they are summed with other potentials.
- The finger motions are generally fast, with small range of motion, thus the amplitude of finger-motion-related surface myoelectric potentials is minute and of low S/N ratio.
- Considerable attention is required to control SEMG-based prostheses, often resulting in fatigue.

However, newer publications show advances in the field. In a paper titled *Surface EMG in advanced hand prosthetics* [8] machine learning together with a simple downsampling algorithm are proved to be an effective approach to classify, in real time, finger movements as well as control finger force of a highly dexterous robotic hand. The system determines the type of grasp a human subject is willing to use, and the required amount of force involved. Regarding the exact decoding of the position of the fingers using SEMG there is not much literature excepting [9]. In this paper from 2008 the results show that, although the general trend of finger movement can be captured using SEMG, the predicted output is still somewhat noisy and improvements on the overall decoding accuracy and noise reduction are necessary.

While the SEMG technology keeps evolving different approaches are being looked into. In [7] accelerometers are placed in the forearm to collect the finger motion related mechanical vibration patterns. Finger movements are afterwards classified using a template matching

method.

The use of US images to identify finger movements is another alternative and object of this thesis. Publications like [2], [10], [11] and [12] represent the most advanced studies employing this technique. The first two of them are the result of the work carried out at the DLR. Features extracted from US images are matched to finger positions via linear regression. Six DOF as well as multi-finger movements are targeted. The resulting regression matrix is later used to produce the prediction based on the incoming images. In [11] and [12] US images are used in conjunction with sEMG to control a powered prosthesis with one DOF.

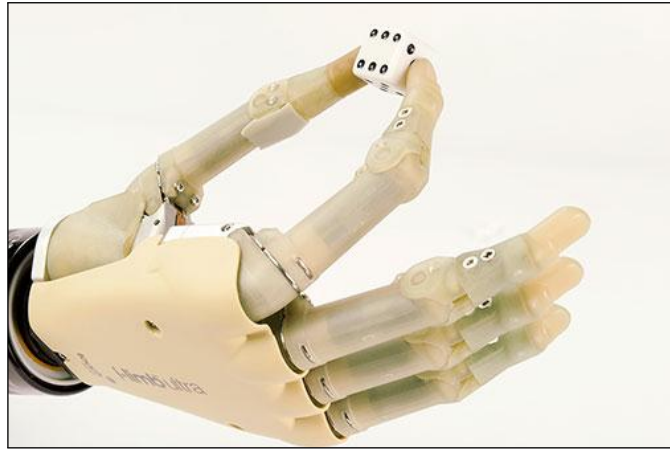


Figure 2.1: i-limb ultra, active prosthetic hand from Touch Bionics [13]

3

Problem analysis

3.1 Problem description

As the title of this document suggests the goal of this project is to produce an online accurate prediction of the angular position of the fingers of the human hand based on a stream of ultrasound images from the forearm. This idea stems from the fact that ultrasound image features of the forearm are linearly related to finger positions, as stated in [2].

Initially only single finger movements are going to be targeted. More precisely the experiments will deal with the following six movements: pinkie flexion-extension, ring flexion-extension, middle flexion-extension, index flexion-extension, thumb adduction-abduction and thumb rotation. All the mentioned finger movements are displayed in figure 3.1 together with the rest position of the hand.

A patient should be able to sit in front of the system, attach the probe of the US machine to the arm and, by means of a Graphical User Interface (GUI), start the application, calibrate all necessary parameters and run the prediction for as long as he wants. The prediction needs to be robust and do not deteriorate over time. To achieve this certain external factors will need to be compensated (being the movements of the probe with respect of the arm the most dangerous of them all). Both hardware and software mechanisms should be implemented in order to maintain the conditions of the experiment stable.

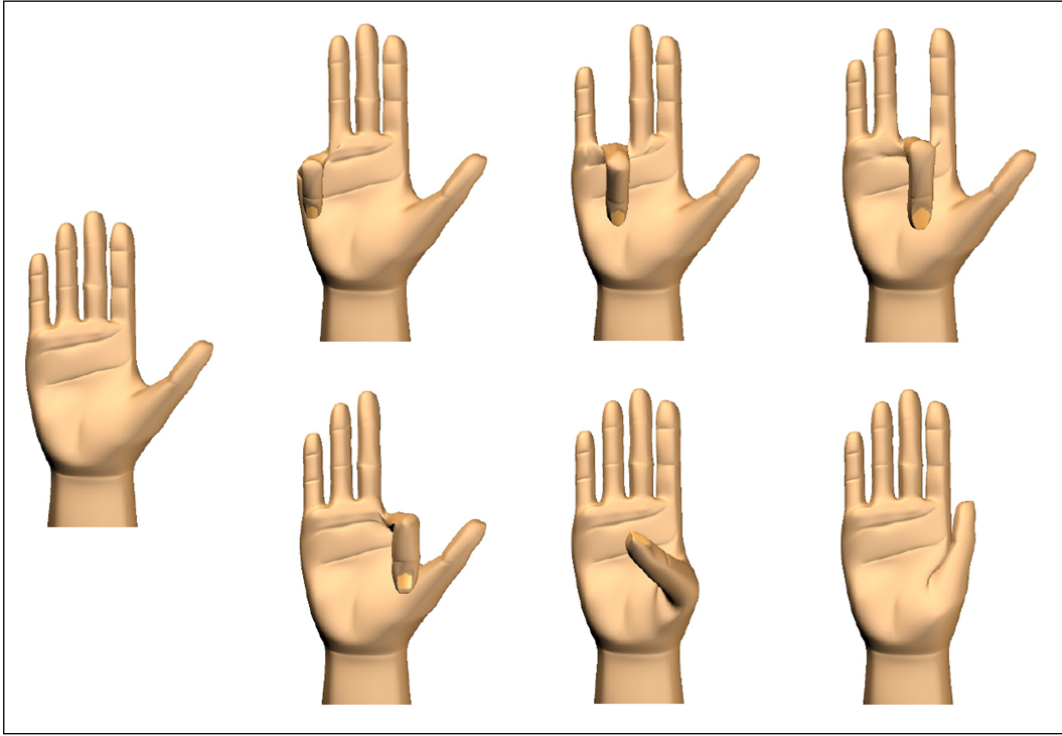


Figure 3.1: Finger movements to be predicted

3.2 General approach

The body of each person is different and because of that it is impossible to prepare a system that would work out-of-the-box with different subjects. Therefore, the first step will always be to tell the system how to interpret the US images, in other words, to train the system.

During the *training phase* the patient is asked to mimic the movements of a hand shown on the screen (stimulus). All the desired movements to be predicted should be included in the stimulus. While the patient mimics the stimulus two different sets of data are being captured: US images of the forearm and the real position of the fingers of the hand. By means of a regression analysis the US images are matched to the positions.

Once enough data has been gathered the training ends and the *prediction phase* begins. US images are fed into the system, which uses the knowledge gathered during the training phase to decode the images and produce an estimation of the position of the fingers. This basic idea is displayed in the shape of a flow diagram in figure 3.2.

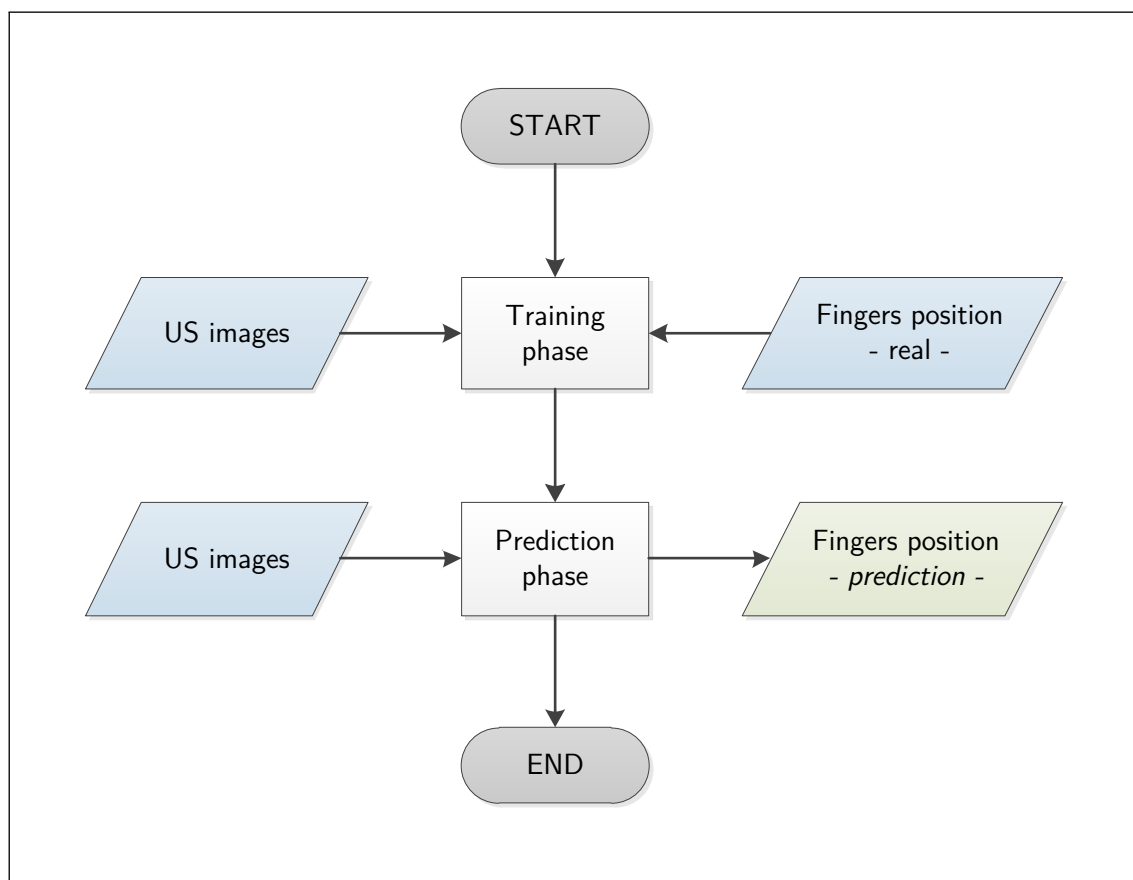


Figure 3.2: Basic approach to the solution

3.3 Previous work

Following the path set up by [2] Emanuel Zarka joined the DLR in 2011 to write his Master Thesis, which was titled *Prediction of finger movements using ultrasound images* [14]. Zarka's work constitutes the natural predecessor of this document and therefore its analysis is necessary in order to clarify the true starting point of this master thesis.

During his time at the DLR Zarka put together all the necessary hardware elements and integrated their functionality into a C++ application. The system would gather images from the portable US machine, extract certain features from them and store these features on the disk. The real position of the fingers was captured by means of another piece of hardware and likewise stored to the disk. Once all the data was on the disk a Matlab application would open, load the data, process it and finally produce a regression matrix and store it on the disk in the shape of a text file. The C++ application would then load this regression matrix from the text file and use it in the prediction phase to estimate the position of the fingers.

To compensate external factors like the shifting of the probe of the US machine along the

arm a simple technique based on *optical flow* was implemented. The system would track whenever the hand of the patient was back in the rest position, compare it with a frame gathered at the beginning of the experiment and modify accordingly the way the features were extracted from the images. The disadvantage of this method is that it forces the user to move the hand to the resting position at regular intervals, which somehow destroys the user experience.

Being a new project as it was, the main target was to prove the real feasibility of the project. Because of that the analysis of the results was done extrictly offline. All the data gathered would be divided into training set (up to half the data size) and testing set and then the errors would be computed.

This previous stage of the project ended with an experiment on an amputee which yielded negative results. The physical setup was considered the biggest responsible of this. The original plan was to have the amputee run the experiment the same way the healthy subjects used to. The arm would lay relaxed on the table with the palm of the hand facing up. The probe would then be held and pressed to the arm by a drill holder. However, the patient soon declared that he was uncomfortable in that position and unable to perform the required movements. A new setup had to be improvised, having this a big impact on the results.

3.4 Goals

The improvements projected for the system during this thesis are the following:

- **Redesign the whole system in C#**

C# is a programming language that provides rapid development times and very high code readability. One of the targets will be to develop a modular and more legible code, making it easier for future developers to understand and to use. A GUI is expected in order to control the program execution, the different parameters of the experiment and also provide the user with visual feedback of what is happening.

- **Implement a more dynamic training system: online training**

The whole system needs to be more flexible, allowing the user to switch back and forth between the training and prediction phases. The training phase will no longer have a fixed duration. Instead, it will end when the user decides the prediction is accurate enough.

- **Online synchronization of the data gathered from the different devices**

The old system stored all the information gathered from the different devices with a time-stamp on the disk. The data synchronization was done exclusively offline. Interpolation of the data was needed because the devices provide data at different

frequencies. In the new system the data will not be stored on the disk and therefore a different synchronization procedure is needed.

- **Make the system stable over time**

Hardware and/or software solutions will be required in order to avoid a decay in the quality of the prediction over time. Previous studies have pointed to the relative movements of the probe of the US machine with respect to the arm as the main cause of this decay.

- **Test the performance of the system on several test objects**

The objective is to obtain a real estimation of how good the final system is.

4

Theoretical framework

4.1 Ultrasonography

Ultrasonography can be described as a process that uses the reflection of high-frequency sound waves to make an image of structures deep within the body. Ultrasounds are one of the most widely used imaging technologies in medicine. It is portable, free of radiation risk, and relatively inexpensive when compared with other imaging modalities, such as magnetic resonance and computed tomography. Furthermore, US images are tomographic, i.e., offering a cross-sectional view of anatomical structures. The images can be acquired in real-time, thus providing instantaneous visual guidance for many interventional procedures including those for regional anesthesia and pain management. [15]

In this section some of the fundamental principles and physics of the ultrasonography are described in order to acquire a basic understanding of the technology.

4.1.1 Sound and wave theory

Sound is a form of energy. It is a pressure wave, created by a mechanical action, and is therefore called a mechanical wave. Sound is produced when a vibrating source causes the molecules of a medium to move back and forth. This backward and forward movement of the molecules creates waves of sound energy that travel, or propagate, through the medium.

A medium is any form of matter: solid, liquid, or gas. Sound requires a medium in which to propagate; therefore, it cannot travel in a vacuum.

When sound energy propagates through a medium, it does so in longitudinal waves, meaning that the molecules of the medium vibrate back and forth in the same direction that the wave is traveling. In summary, sound is a mechanical, longitudinal wave. Longitudinal waves should not be confused with transverse waves where molecules in a medium vibrate at 90° to the direction of the traveling wave. [16]

4.1.1.1 Acoustic Variables

Acoustic variables are changes that occur within a medium as a result of sound traveling through that medium. The three primary acoustic variables are **pressure**, **density** and **distance**. As stated before, when sound energy propagates through a medium, it causes the molecules to move back and forth. Each back and forth movement completes one wave or one cycle of movement. Each cycle consists of two parts: a *compression*, where the molecules are pushed closer together, and a *rarefaction*, where they are spread wider apart. The molecules, as they are squeezed together and separated, cause changes in the pressure within the medium. Similarly, molecules undergoing compression and rarefaction show variations in density.

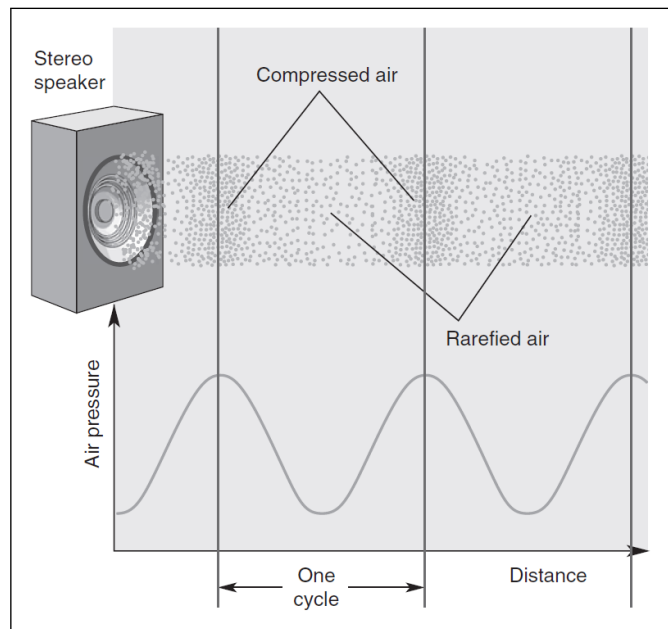


Figure 4.1: Production of sound by variations in air pressure [16]

Figure 4.1 exemplifies the production of sound by variations in air pressure. When the paper cone of a stereo speaker pushes out, it compresses the air, represented by peaks on the graph; when the cone pulls in, it rarefies the air, represented by troughs on the graph.

If the push and pull are periodic, there is also a periodic variation in the air pressure, as shown in the graph. The distance between successive compressed (high-pressure) patches of air is one cycle of the sound (indicated by the vertical lines). The sound wave propagates away from the speaker at the speed of sound. [16]

4.1.1.2 Parameters of sound

Sound waves have several parameters that may be utilized to describe them. Parameters of sound waves include the period, frequency, amplitude, power, intensity, propagation speed and wavelength. In this chapter the relationship that these parameters have with each other is discussed.

Period and frequency Period (T) is defined as the time it takes for one cycle to occur and measured in seconds (s). Frequency (f) is defined as the number of cycles per second and measured in hertz (Hz). Frequency and period are inversely related.

$$T = \frac{1}{f} \quad (4.1)$$

Propagation speed Propagation speed (c) is defined as the speed at which a sound wave travels through a medium. All sound, regardless of its frequency, travels at the same speed through any particular medium. Therefore, a 20 Hz sound wave and a 20 MHz sound wave travel at the same speed in a given medium. Propagation speeds tend to be the fastest in solids, such as bone, and slowest in gases or gas-containing structures, such as the lungs (table 4.1). In the body, sound travels at slightly different speeds through the various organs and tissues. The units for propagation speed are meters per second (m/s). The average speed of sound in all soft tissue is considered to be 1540 m/s. This number was derived by averaging all of the actual propagation speeds of the tissues in the body.

Medium	Propagation speed (m/s)
Air	330
Lungs	660
Water	1480
Soft tissue	1540
Liver	1555
Blood	1560
Bone	4080

Table 4.1: Media and their propagation speeds [16]

The propagation speed of sound in a medium is influenced by two properties: the **stiffness (elasticity)** and the **density (inertia)** of the medium. Stiffness is defined as the ability of an object to resist compression and relates to the hardness of a medium. Stiffness and propagation speed are directly related: the stiffer the medium, the faster the propagation speed. Conversely, density, which can be defined as the amount of mass in an object, is inversely related to propagation speed. [16]

$$\text{Propagation speed} = \frac{\text{Elasticity}}{\text{Density}} \quad c = \frac{e}{\rho} \quad (4.2)$$

Wavelength The length of a single cycle of sound is called the wavelength (λ). It is the distance from the beginning of a cycle to the end of that cycle and it is measured in meters (m). Like period, wavelength and frequency are inversely related. However, the wavelength of a sound wave is also influenced by the propagation speed of the medium in which it is traveling. The faster the propagation speed, the longer the wavelength. In diagnostic imaging, because the average propagation speed of sound in soft tissue is treated as a constant of 1540 m/s, any change in the wavelength would be related only to changes in the frequency. Wavelength is in essence equal to the propagation speed divided by the frequency with $c = 1540$ m/s. [16]

$$f = \frac{c}{\lambda} \quad (4.3)$$

Amplitude, power and intensity Amplitude, power, and intensity all relate to the size or strength of the sound wave. All three of these decrease as sound travels through a medium. Amplitude (A) is defined as the maximum or minimum deviation of an acoustic variable from the average value of that variable. When amplitude is discussed in ultrasound physics, it is commonly the pressure amplitude that is being referenced. The units of amplitude are therefore Pascals (Pa). Power (P) is defined as the rate at which work is performed or energy is transmitted. As a sound wave travels through the body, it loses some of its energy. Therefore, power decreases as the sound wave moves through the body. The power of a sound wave is typically described in units of watts (W). Power is proportional to the amplitude squared. The intensity (I) of a sound wave is defined as the power of the wave divided by the area (a) over which it is spread, or the energy per unit area and measured in units of watts per centimeter squared (W/cm^2). [16]

Impedance Any medium through which sound is traveling will offer some amount of resistance to the sound. This resistance to the propagation of sound through a medium is

called impedance (z). The amount of impedance depends on the density (ρ) and the propagation speed (c) of the medium. Keep in mind that the density and stiffness are the controlling factors of propagation speed. Impedance is measured in units called Rayls.

$$z = \rho c \quad (4.4)$$

There are slight variations in the density of the various tissues in the body just as there are slight variations in the propagation speed. Recall that 1540 m/s is used as the average speed of sound in all soft tissue. As a result, many of the tissues will have different impedance values. It is these variations in impedance that help create reflections at the interface between adjacent tissues. Assuming the beam strikes the interface at a 90° angle and there exists a large impedance difference between two tissues, there will be a strong reflection and a well-defined boundary displayed on the imaging screen. If the impedance difference between two media is more subtle, there will be a weaker reflection. If the impedances are the same, no reflection occurs. [16]

Body Tissue	Acoustic impedance (10^6 Rayls)
Air	0.0004
Lung	0.18
Fat	1.34
Liver	1.65
Blood	1.65
Kidney	1.63
Muscle	1.71
Bone	7.8

Table 4.2: Acoustic impedances of different body tissues and organs [15]

4.1.2 Ultrasound production

The generation of an ultrasonic wave impulse is achieved through the piezoelectric effect (pressure electric effect). This phenomena was first noted by the Curies at the turn of the century. In simple terms, the piezoelectric effect is the phenomenon that occurs when crystalline material vibrates at given frequency when an alternating current is applied. The vibration consists of expansion and contraction of the material. Conversely, if an external ultrasonic wave hits the crystal, the crystal will vibrate and generate an electric current across the dipole. In essence, the piezoelectric crystal acts both as a speaker and as a microphone. In medical ultrasound, the crystals are placed in a sealed transducer, which comes in contact with the patient. Piezoelectric crystals in diagnostic ultrasound are used in two different modes: continuous and pulsed echo. **Continuous mode** is generated when

a constant current is placed across the crystal. This mode is used in Doppler sonography to detect and measure blood flow. In continuous mode, one crystal generates the signal, while another acts as receiver. **Pulsed echo** mode is used for all other ultrasonic applications. In this mode the crystal generates an ultrasonic signal for a given period and then acts as a receiver for a period of time, acting as both signal generator and receiver. [17]

The machine must time how long it takes for a pulse of sound to reach the reflector in order to appropriately display anatomy on the monitor. If the transducer sends out a pulse before it receives the last one, it is unable to recognize where the echo originated, and therefore, cannot display it correctly on the monitor. This is referred to as depth ambiguity. [16]

4.1.3 Transducers

Modern ultrasound equipment utilizes real-time, or automatic scanning, to obtain diagnostic images of the body. With real-time scanning, the transducer is responsible for sending out scan lines across a defined plane. Images are produced when an ultrasound beam is swept across that plane. Pulses of ultrasound are sent out and produce scan lines. All of the scan lines, when placed next to each other, form an image that is called a frame.

There are two methods of sending out scan lines to form an image using real-time: mechanical scanning (via mechanical transducers) and electronic scanning (via electronic transducers). Both of these methods provide a means for sweeping the ultrasound beam through the tissue repeatedly and rapidly.

4.1.3.1 Mechanical Transducers

Mechanical scanheads are not commonly utilized in today's busy sonography departments. These transducers typically had one or more piezoelectric elements connected to a motor, or a fixed element with a mirror connected to a motor. The motor steered the element, or a mirror, to produce the scan lines that made up the image. This produced a sector image pattern. These transducers had fixed frequency and fixed focus. That is, in order to change the frequency or the location of the focal zone, one had to change the entire scanhead. Focusing of the beam was achieved by either the shape of the element or the use of a lens. The major advantages of the mechanical transducer were that they were inexpensive and typically had a small footprint (the portion of the transducer that is in contact with the patient's skin). Unfortunately, they were fragile and their mechanical elements were easily broken. [16]

4.1.3.2 Electronic Transducers

Electronic scanning is performed with transducers that have multiple active elements. This is referred to as an array. An array is formed by taking a single slab of PZT and slicing it down into multiple subelements. Each subelement is connected to a wire, so it may fire independently (figure 4.2). The system can selectively excite the elements as needed to shape and steer the beam. With most array transducers, no motors are needed for beam steering. Arrays may be either sequenced or phased and can produce various image shapes. [16]

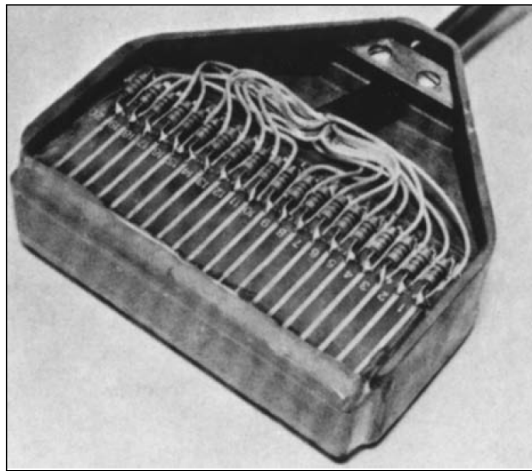


Figure 4.2: Wires of a US transducer. Note that each element is connected by a wire [16]

Linear Sequenced Array The linear sequenced array, also referred to as the linear sequential array or linear array, is a transducer that is often used in vascular or small parts imaging. This transducer produces a rectangular shaped image. With the linear sequenced array, the elements are arranged in a line, next to each other, but are fired in small groups in sequence. For example, the elements are not fired (1,2,3,4,5) but are fired (1,2,3)(4,5,6)(7,8,9)... Linear sequenced arrays do not need any beam steering to produce a rectangular image. However, should beam steering be needed, whether for Doppler or to create a vector image, the beam can be electronically steered. The linear sequenced array available at the DLR as well as its footprint are displayed in figure 4.3. [16]

Curved Sequenced Array The curved sequenced array transducer, also referred to as a convex, curvilinear, or curved sequential array, is based on the same technology as that of the linear sequenced array but with a curved face. As with the linear sequenced array, the elements are fired in groups. [16]

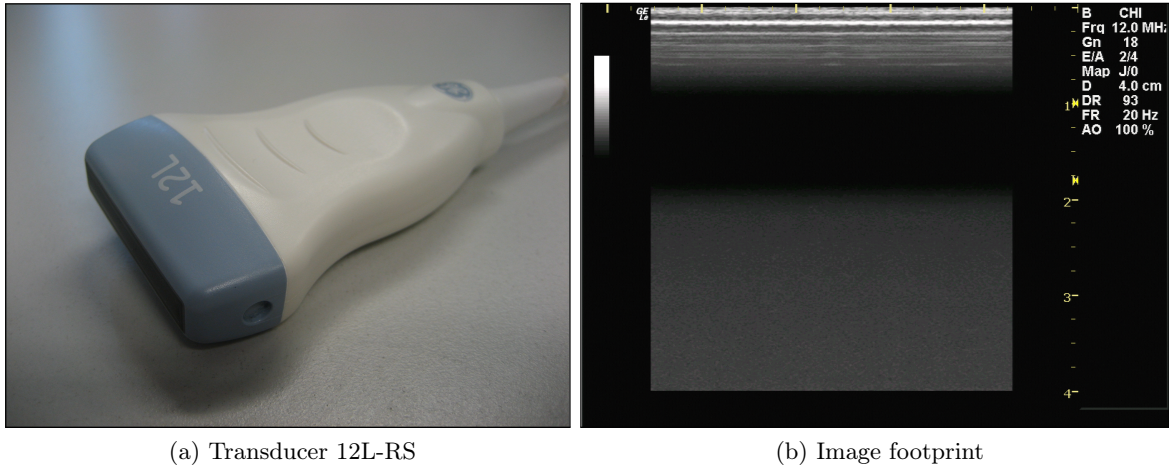


Figure 4.3: Linear sequenced array available at the DLR

Linear Phased Arrays The linear phased array, also referred to as simply a phased array, is more commonly known as a sector or vector transducer. This probe typically has a small footprint and is used for cardiac imaging, neonatal brain imaging, with some endocavitary transducers, and any other application where a sector image shape is desired. In order to create a sector image, electronic steering is needed for every scan line. Naturally, the phased array uses phasing to steer and focus the beam. Phasing is changing the timing of the shocking of the elements in order to shape and steer the beam. All arrays are phased focused. That is, all of the array transducers mentioned in this section use phasing to control the focusing in the scan plane. Phasing provides the sonographer the ability to control the depth of the focal zone in the scan plane. [16]

4.1.4 Display modes

There are different modes used in ultrasound imaging for displaying the return echo information on the display. A general view of how they work is displayed in figure 4.4

4.1.4.1 A-Mode

One of the original methods of displaying the return echo information was a display similar to an oscilloscope, where the depth was represented along the x-axis and the strength of the reflector was represented as a “spike” along the y-axis. A pulse of sound was sent out to create one scan line of information, which contained the depth and amplitude of the reflectors. No image was generated, only a set of spikes representing the amplitude of reflectors and their depth. This display method is called amplitude mode or A-mode, and

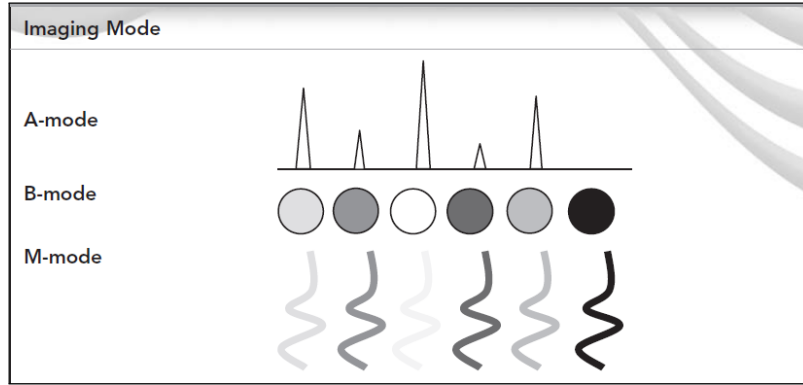


Figure 4.4: Ultrasound imaging modes [16]

it is still utilized in echocardiography and in dedicated ophthalmology/sonography units. [16]

4.1.4.2 B-Mode

Brightness mode, or B-mode imaging, displays the return echoes as dots of varying brightnesses. The brightness of the dot represents the strength of the return echo. Modern equipment uses a white dot on a black background. The brighter the dot, the stronger the return echo. Very strong reflectors will be white or almost white (hyperechoic), weak reflectors will be a darker shade of gray (hypoechoic), and if there is no return echo information at all, then all that is seen at that location is black (anechoic). That is to say, that a black space on the screen is absence of a return echo. This is why a full bladder appears anechoic. Simple fluids, such as water or urine, do not reflect much of the sound wave, so no dot is painted on the display in that area. The brightness of the dot representing the amplitude of the return echo corresponds to the height of the spike on the A-mode display.

The B-mode image is made up of many scan lines stacked next to each other. Each scan line is made up of one or more pulses of sound. In order for the machine to know where to place the dots on the screen, it has to know where the return echoes came from. In order to determine where the echo came from, the time it takes for the sound to reach the reflector and return must be known. This is summed up by the range equation, which states that the distance to the reflector (d , in millimeters) is equal to the propagation speed (c) multiplied by the round-trip time (t , in microseconds), or time to the reflector and back. [16]

$$d = \frac{c \times t}{2} \quad (4.5)$$



Figure 4.5: B-mode image of the upper abdomen [16]

4.1.4.3 M-Mode

With B-mode imaging, we are usually interested in the anatomy represented in the whole image. However, there are times when we are more concerned with the movement of the reflectors and not the anatomy. M-mode, or motion mode, is used in these instances when documentation of the movement of a reflector is needed, such as looking at the motion of a heart valve or myocardial wall thickness during systole and diastole. M-mode is often used in obstetrics and in cardiac applications. With M-mode imaging, the motion of the reflectors along a single scan line is analyzed. The M-mode tracing is one scan line represented over time with depth along the y-axis and time along the x-axis. This is sometimes referred to as “ice-pick” imaging because of the very narrow field-of-view. [16]

4.1.5 Ultrasound-tissue interaction

As US waves travel through tissues, they are partly transmitted to deeper structures, partly reflected back to the transducer as echoes, partly scattered, and partly transformed to heat. For imaging purposes, we are mostly interested in the echoes reflected back to the transducer. As seen before, the amount of echo returned after hitting a tissue interface is determined by a tissue property called acoustic impedance (table 4.2).

The intensity of a reflected echo is proportional to the difference (or mismatch) in acoustic impedances between two mediums. If two tissues have identical acoustic impedance, no echo is generated. Interfaces between soft tissues of similar acoustic impedances usually generate low-intensity echoes. Conversely interfaces between soft tissue and bone or the lung generate very strong echoes due to a large acoustic impedance gradient.

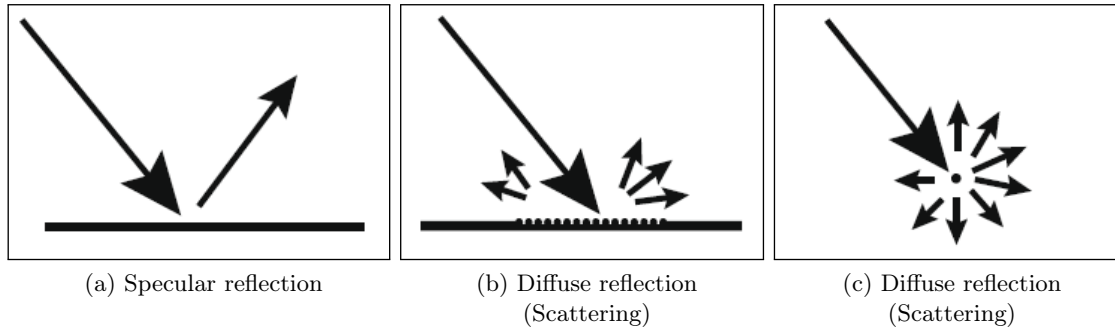


Figure 4.6: Different types of ultrasound wave-tissue interactions [15]

When an incident ultrasound pulse encounters a large, smooth interface of two body tissues with different acoustic impedances, the sound energy is reflected back to the transducer. This type of reflection is called **specular reflection**, and the echo intensity generated is proportional to the acoustic impedance gradient between the two mediums.

If the incident US beam reaches the linear interface at 90° , almost all of the generated echo will travel back to the transducer. However, if the angle of incidence with the specular boundary is less than 90° , the echo will not return to the transducer, but rather be reflected at an angle equal to the angle of incidence (just like visible light reflecting in a mirror). The returning echo will potentially miss the transducer and not be detected. **Refraction** refers to a change in the direction of sound transmission after hitting an interface of two tissues with different speeds of sound transmission. In this instance, because the sound frequency is constant, the wavelength has to change to accommodate the difference in the speed of sound transmission in the two tissues. This results in a redirection of the sound pulse as it passes through the interface. Refraction is one of the important causes of incorrect localization of a structure on an ultrasound image.

If the ultrasound pulse encounters reflectors whose dimensions are smaller than the ultrasound wavelength, or when the pulse encounters a rough, irregular tissue interface, **scattering** occurs. In this case, echoes reflected through a wide range of angles result in reduction in echo intensity. However, the positive result of scattering is the return of some echo to the transducer regardless of the angle of the incident pulse. Most biologic tissues appear in US images as though they are filled with tiny scattering structures. The speckle signal that provides the visible texture in organs like the liver or muscle is a result of interface between multiple scattered echoes produced within the volume of the incident ultrasound pulse.

As US pulses travel through tissue, their intensity is reduced or attenuated. This attenuation is the result of reflection and scattering and also of friction-like losses. These losses result from the induced oscillatory tissue motion produced by the pulse, which causes conversion of energy from the original mechanical form into heat. This energy loss to lo-

calized heating is referred to as absorption and is the most important contributor to US attenuation. Longer path length and higher frequency waves result in greater attenuation. Attenuation also varies among body tissues, with the highest degree in bone, less in muscle and solid organs, and lowest in blood for any given frequency. All ultrasound equipment intrinsically compensates for an expected average degree of attenuation by automatically increasing the gain. [15]

4.2 Hand and forearm anatomy

This section aims to give an overview of all the anatomical aspects involved with the project at hand. In particular, it is interesting to understand how the forearm is internally structured and how the fingers of the hand move. With this information it will be possible to interpret physically the US images seen in the previous section and also to understand how the 3D Hand Model used in this thesis works.

4.2.1 Terminology

The first thing that needs to be clarified in this section is the terminology relative to directions and movements that can be found in medical texts. A summary of this terminology is displayed in tables 4.3 and 4.4.

Direction	Term	Meaning
<i>Relative to front or back of the body</i>	Anterior	In front of, toward the front surface
	Posterior	In back of, toward the back surface
	Dorsal	At the back side of the human body
	Ventral	At the belly side of the human body
<i>Relative to the midline or center of the body</i>	Medial	Toward the midline of the body
	Lateral	Away from the midline of the body
	Deep	On the inside, underneath another structure
	Superficial	On the outside
<i>Relative to point of attachment of the appendage</i>	Proximal	Closest to point of attachment to trunk
	Distal	Furthest from point of attachment to trunk

Table 4.3: Anatomic terminology relative to directions [18]

Movement	Description
<i>Angular motion</i>	The angle between articulating bones increases or decreases
Flexion	The angle between articulating bones decreases
Extension	The angle between articulating bones increases
Hyperextension	Extension movement continues past the anatomic position
Abduction	Movement of a bone away from the midline
Adduction	Movement of a bone toward the midline
<i>Rotational Motion</i>	A bone pivots around its own longitudinal axis
Pronation	Rotation of the forearm whereby the palm is turned posteriorly
Supination	Rotation of the forearm whereby the palm is turned anteriorly

Table 4.4: Anatomic terminology relative to movements [18]

4.2.2 Forearm

The forearm is the structure and distal region of the upper limb, between the elbow and the wrist. The term forearm is used in anatomy to distinguish it from the arm, a word which is most often used to describe the entire appendage of the upper limb, but in anatomy, technically, it means only the region of the upper arm, whereas the lower arm is called the forearm.

The forearm contains two long bones, the radius and the ulna, forming the radioulnar joint. The interosseous membrane connects these bones. Ultimately, the forearm is covered by skin, the anterior surface usually being less hairy than the posterior surface.

The forearm contains many muscles, including the flexors and extensors of the digits, a flexor of the elbow (brachioradialis), and pronators and supinators that turn the hand to face down or upwards, respectively. In cross-section the forearm can be divided into two fascial compartments. The posterior compartment contains the extensors of the hands, which are supplied by the radial nerve. The anterior compartment contains the flexors, and is mainly supplied by the median nerve. The ulnar nerve also runs the length of the forearm.

The radial and ulnar arteries, and their branches, supply the blood to the forearm. These usually run on the anterior face of the radius and ulna down the whole forearm. The main superficial veins of the forearm are the cephalic, median antebrachial and the basilic vein. These veins can be used for cannularisation or venipuncture, although the cubital fossa is a preferred site for getting blood. [19]

The skeletal and muscular structure of the arm is displayed in figures 4.7, 4.8 and 4.9.

4.2.2.1 Forearm muscles that move the wrist joint, hand and fingers

Most muscles in the forearm move the hand at the wrist and/or the fingers. These muscles are called extrinsic muscles of the wrist and hand, because the muscles originate on the forearm, not the wrist or hand. The forearm is bigger near the elbow because the bellies of these forearm muscles form the bulk of this region. Moving toward the wrist, the forearm thins because there are no longer big muscle bellies, but rather the long tendons that project from these muscles.

Deep fascia partitions the forearm muscles into an anterior (flexor) compartment and a posterior (extensor) compartment (figure 4.10). Most of the anterior compartment muscles originate on the medial epicondyle of the humerus via a common flexor tendon. *Muscles in the anterior compartment of the forearm tend to flex the wrist, the metacarpophalangeal (MCP) joints, and/or the interphalangeal (IP) joints of the fingers.* Most of the posterior compartment muscles originate on the lateral epicondyle of the humerus via a common extensor tendon. *Muscles in the posterior compartment of the forearm tend to extend the wrist, the MP joints, and/or the IP joints.*

Note that not all anterior forearm muscles cause flexion. The pronator teres and the pronator quadratus are located in the anterior compartment of the forearm, although their primary function is pronation. Likewise, the supinator muscle is in the posterior compartment of the forearm, even though its primary function is supination.

The tendons of forearm muscles typically are surrounded by tendon (synovial) sheaths and held adjacent to the skeletal elements by strong fascial structures. At the wrist, the deep fascia of the forearm forms thickened, fibrous bands termed retinacula. The retinacula help hold the tendons close to the bone and prevent the tendons from “bowstringing” outward. The palmar (anterior) surface of the carpal bones is covered by the flexor retinaculum. Flexor tendons of the digits and the median nerve pass through the tight space between the carpal bones and the flexor retinaculum, which is called the carpal tunnel. The extensor retinaculum is superficial to the dorsal surface of the carpal bones. Extensor tendons of the wrist and digits pass between the carpal bones and the extensor retinaculum.

The muscles of the anterior compartment of the forearm may be subdivided into a superficial layer, an intermediate layer and a deep layer. The superficial and intermediate muscles originate from the common flexor tendon that attaches to the medial epicondyle of the humerus. The deep layer of muscles originates directly on the forearm bones.

The superficial layer of anterior forearm muscles is arranged from the lateral to the medial surface of the forearm in the following order: pronator teres, flexor carpi radialis, palmaris longus, and flexor carpi ulnaris.

The flexor carpi radialis extends diagonally across the anterior surface of the forearm. Its tendon is prominent on the lateral side of the forearm. This muscle flexes the wrist and abducts the hand at the wrist. The palmaris longus is absent in approximately 10% of all individuals. This narrow, superficial muscle on the anterior surface of the forearm weakly assists in wrist flexion. On the anteromedial side of the forearm, the flexor carpi ulnaris is positioned to both flex the wrist and adduct the hand at the wrist.

The intermediate layer in the anterior compartment of the forearm contains a single muscle, the flexor digitorum superficialis. This muscle splits into four tendons that each insert on the middle phalanges of fingers 2-5 (where 1 is the thumb and 5 the little finger). This muscle crosses over the wrist, MP joints, and PIP (Proximal InterPhalangeal) joints of fingers 2-5; thus, it flexes all of these joints. Since the flexor digitorum superficialis does not cross over the DIP (distal interphalangeal) joints of these fingers, it cannot move the DIP joints.

The deep layer of the forearm anterior compartment muscles includes the flexor pollicis longus (lateral side) and the flexor digitorum profundus (medial side). Deep to both of these muscles is the pronator quadratus muscle.

The flexor pollicis longus attaches to the distal phalanx of the thumb and flexes the MP and IP joints of the thumb. In addition, because this muscle crosses the wrist joint, it can weakly flex the wrist. The flexor digitorum profundus lies deep to the flexor digitorum superficialis. This muscle splits into four tendons that insert on the distal phalanges of fingers 2-5. At the level of the middle phalanges, the tendons of the flexor digitorum superficialis split to allow the flexor digitorum profundus tendons to pass to the tips of the fingers. The flexor digitorum profundus flexes the wrist, MP joints, PIP joints, and DIP joints of fingers 2-5.

Muscles of the posterior compartment of the forearm are primarily wrist and finger extensors. An exception is the supinator, which helps supinate the forearm. The posterior compartment muscles may be subdivided into a superficial layer and a deep layer.

The superficial layer of posterior forearm muscles originates from a common extensor tendon on the lateral epicondyle of the humerus. These muscles are positioned laterally to medially as follows:

- The extensor carpi radialis longus is a long, tapered muscle that is medial to the brachioradialis. It extends the wrist and abducts the hand at the wrist.
- The extensor carpi radialis brevis works synergistically with the extensor carpi radialis longus.
- The extensor digitorum splits into four tendons that insert on the distal phalanges of fingers 2-5. It extends the wrist, MP, PIP and DIP joints of fingers 2-5.

- The extensor digiti minimi attaches to the distal phalanx of finger 5. It works with the extensor digitorum to extend the little finger.
- On the medial surface of the posterior forearm, the extensor carpi ulnaris inserts on the fifth metacarpal bone, where it acts to extend the wrist and adduct the hand.

The deep layer originates directly on the posterior forearm bones and inserts on the wrist or hand bones. These muscles are arranged from lateral to medial in the following order: supinator, abductor pollicis longus, extensor pollicis brevis, extensor pollicis longus, and extensor indicis.

These muscles weakly extend the wrist, and perform the following other functions:

- The abductor pollicis longus inserts on the first metacarpal. It abducts the thumb.
- The extensor pollicis brevis lies immediately medial to the abductor pollicis longus. The extensor pollicis brevis attaches to the proximal phalanx of the thumb and helps extend the MP joint of the thumb.
- The extensor pollicis longus extends the MP and IP joints of the thumb.
- The extensor indicis is the most medial muscle of the deep posterior compartment. It extends the MP, PIP, and DIP joints of the index finger. [18]

A summary of the forearm muscles and their functions can be found in table 4.5.

Figures 4.10 and 4.11, and figures 4.12 and 4.13 provide a comparison of the anatomical distribution and its correspondent US cross section at the middle and distal part of the forearm respectively.

These images are a very good resource for the interpretation of the US images. The muscles that are going to be more active during the experiments are the flexor digitorum profundus and superficialis, the abductor pollicis longus and the extensor indicis, as could be expected by examining the functions of these muscles in table 4.5.

When moving the different fingers during the experiments the probe will need to be placed where the changes in the US images are clearer and more different between fingers. Having an understanding of the underlying structures behind the US images will give an orientation on where to place the probe after a quick examination.

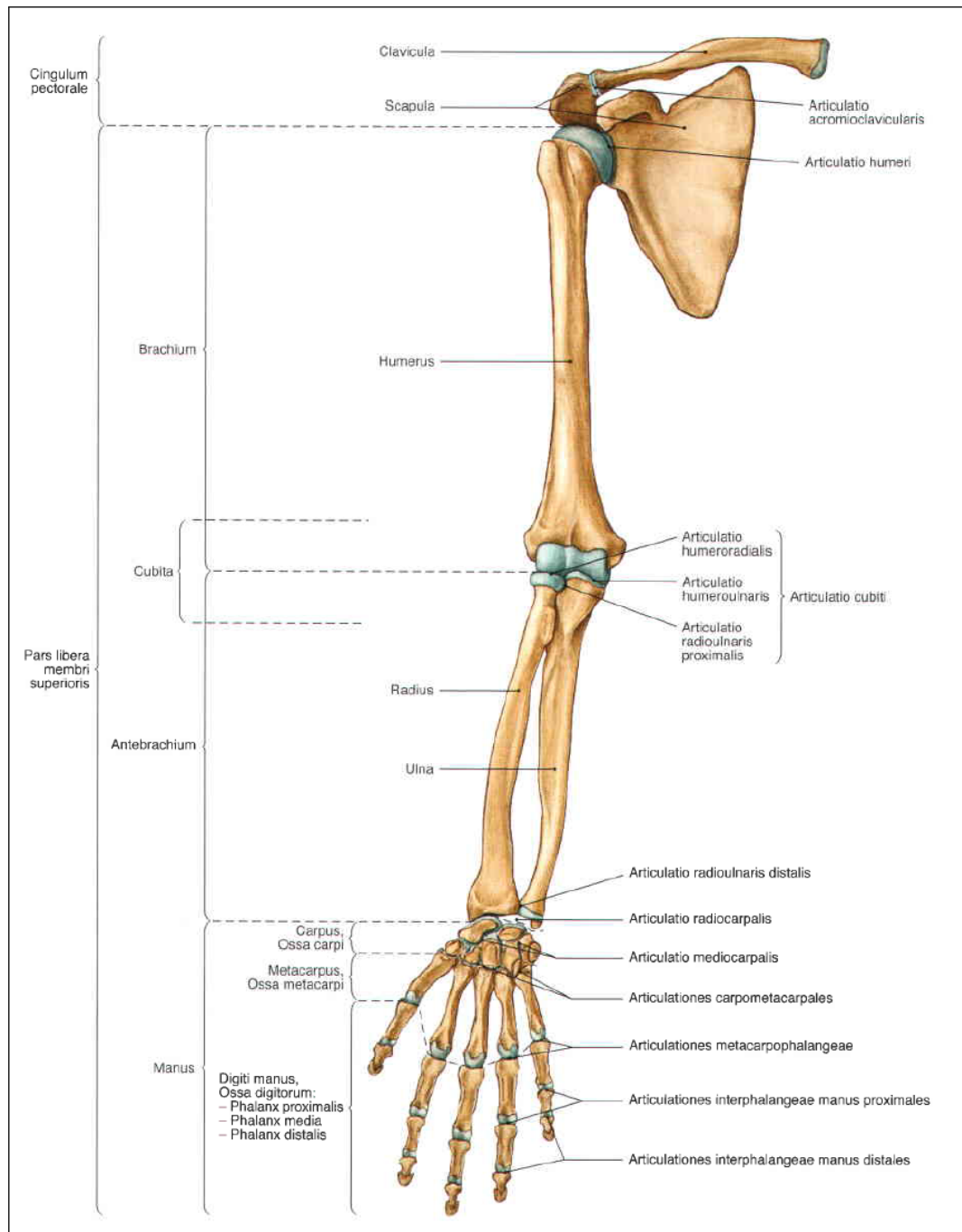


Figure 4.7: Overview of bones and joints of the upper limb [20]

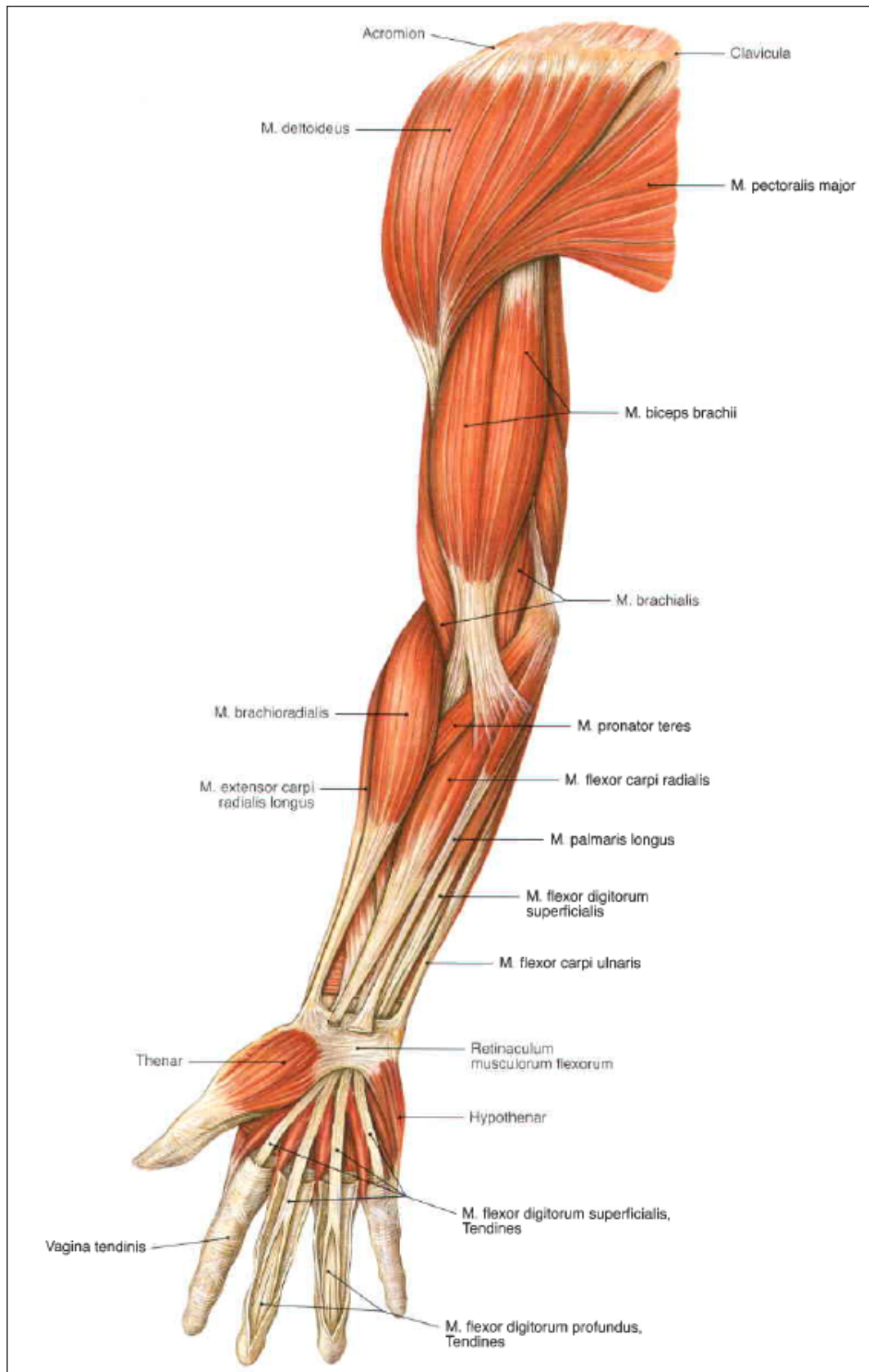


Figure 4.8: Muscles of the flexor aspect of the upper limb [20]

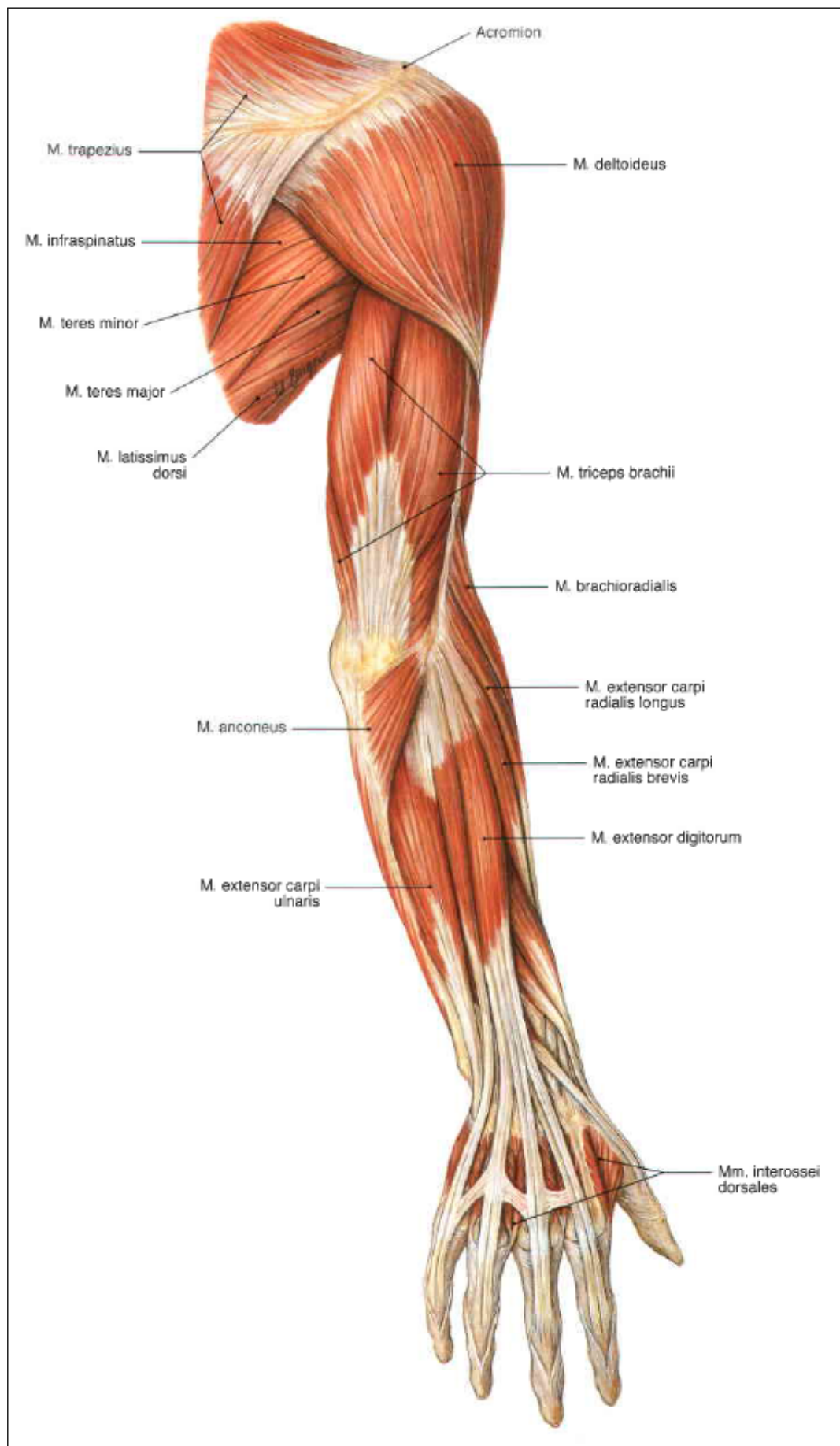


Figure 4.9: Muscles of the extensor aspect of the upper limb [20]

Group/Muscle	Action
<i>ANTERIOR MUSCLES: SUPERFICIAL</i>	
Pronator teres	Pronates forearm
Flexor carpi radialis	Flexes wrist and abducts hand
Palmaris longus	Weak wrist flexor
Flexor carpi ulnaris	Flexes wrist and adducts hand
<i>ANTERIOR MUSCLES: INTERMEDIATE</i>	
Flexor digitorum superficialis	Flexes wrist, 2-5 MP and PIP joints
<i>ANTERIOR MUSCLES: DEEP</i>	
Flexor pollicis longus	Flexes MP, IP joints of thumb, weakly flexes wrist
Flexor digitorum profundus	Flexes wrist, 2-5 MP, PIP and DIP joints
Pronator quadratus	Pronates forearm
<i>POSTERIOR MUSCLES: SUPERFICIAL</i>	
Extensor carpi radialis longus	Extends wrist, abducts hand
Extensor carpi radialis brevis	Extends wrist, abducts hand
Extensor digitorum	Extends wrist and 2-5 MP, PIP, DIP joints
Extensor digiti minimi	Extends wrist, MP, and PIP joints of finger 5
Extensor carpi ulnaris	Extends wrist, adducts hand
<i>POSTERIOR MUSCLES: DEEP</i>	
Abductor pollicis longus	Abducts thumb, extends wrist weakly
Extensor pollicis brevis	Extends MP joints of thumb and wrist weakly
Extensor pollicis longus	Extends MP, IP joints of thumb and wrist weakly
Extensor indicis	Extends 2 MP, PIP, DIP joints and wrist weakly
Supinator	Supinates forearm

Table 4.5: Forearm muscles that move the wrist joint, hand and fingers [18]

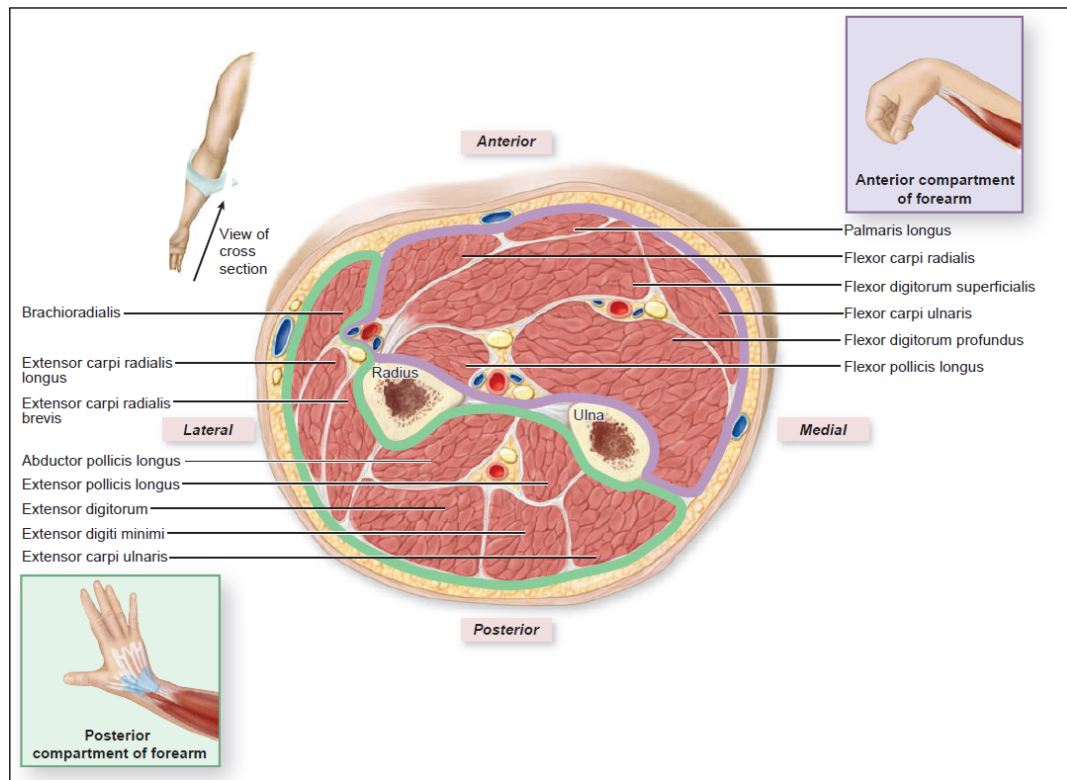


Figure 4.10: Cross-sectional view of the right mid-forearm showing the action muscles [18]

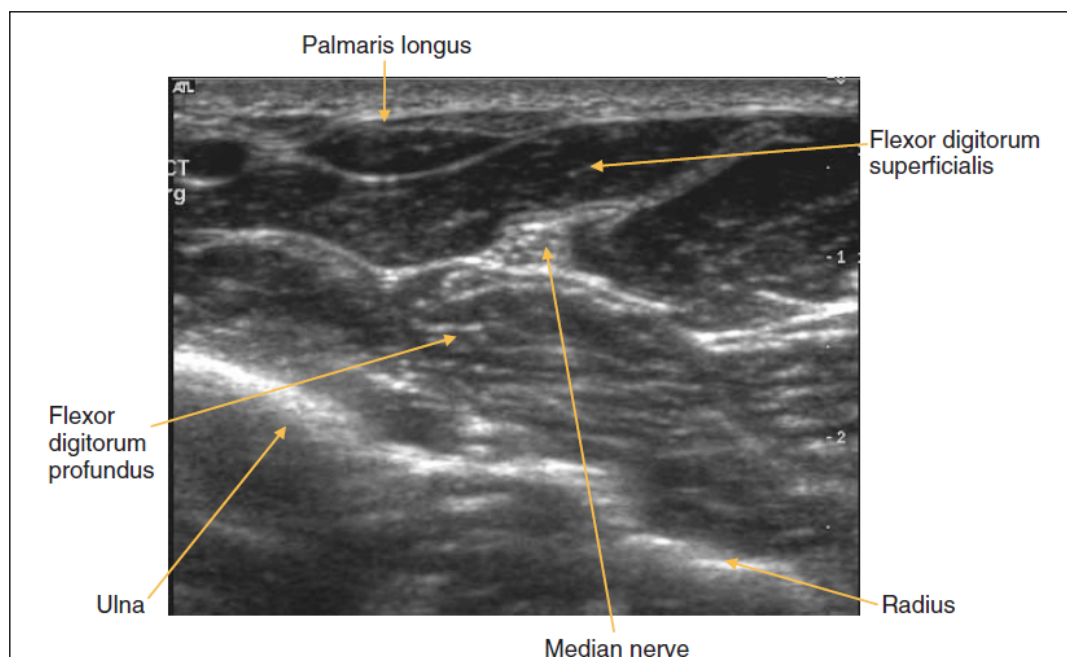


Figure 4.11: Transverse section US imaging of the mid-forearm [21]

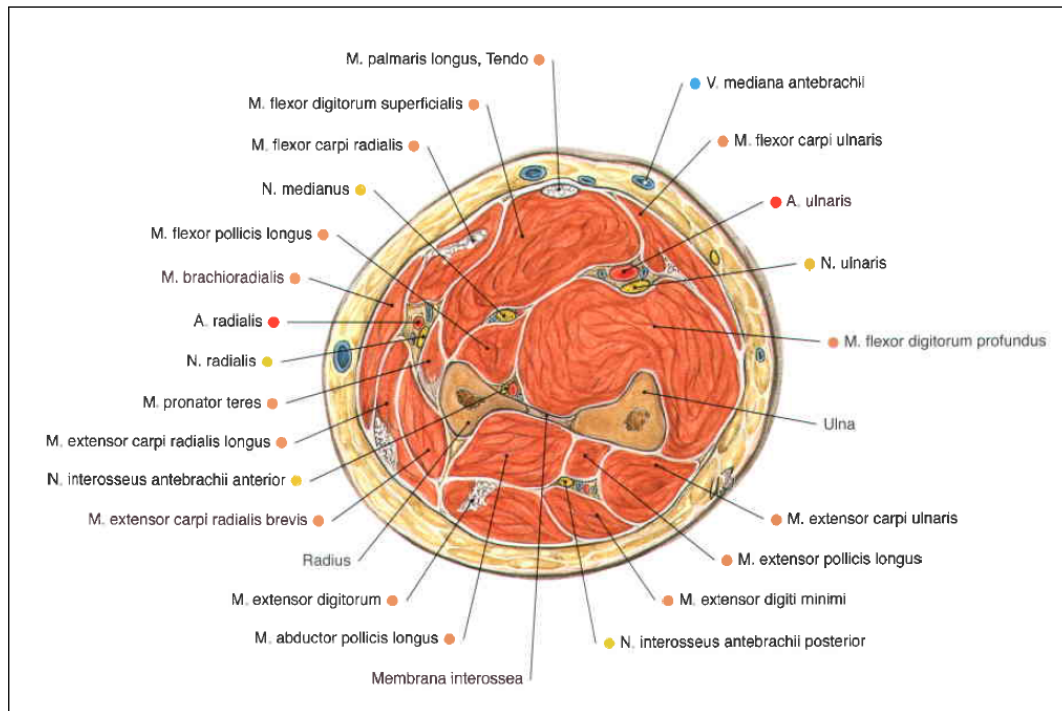


Figure 4.12: Transverse section through the lower third of the forearm [20]

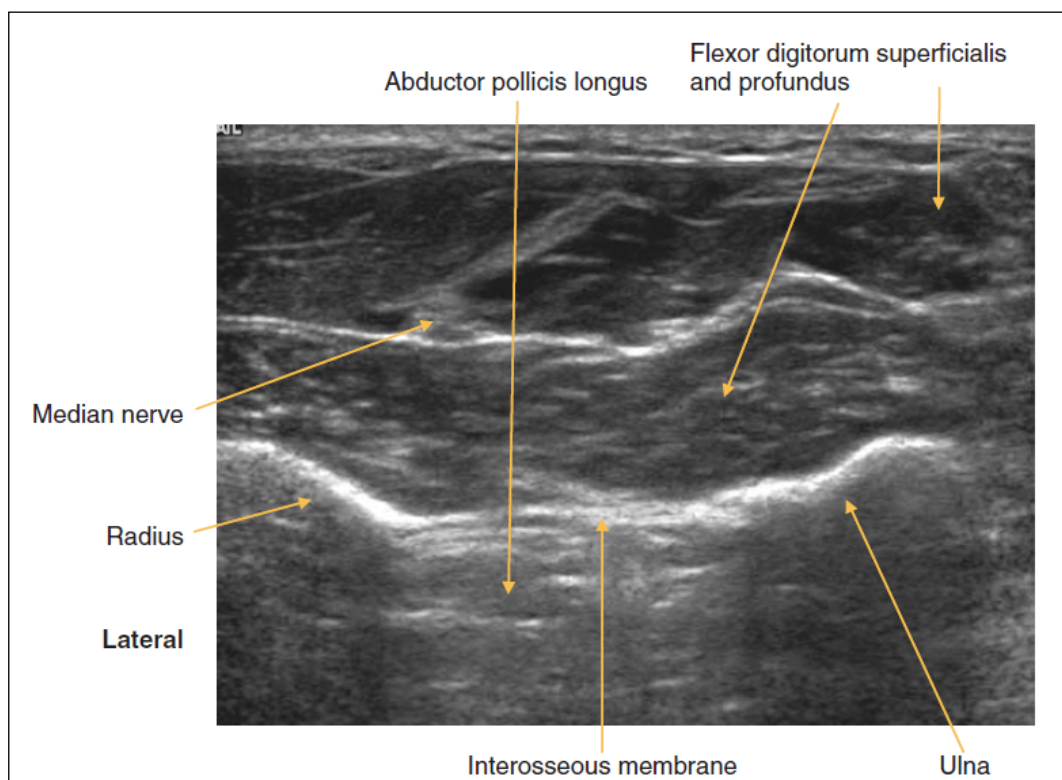


Figure 4.13: Transverse section US imaging of the distal anterior forearm [21]

4.2.3 Hand

A lot can be said and written about the anatomy of the hand. Regarding this thesis it will be important to know which bones compose the hands and how they are articulated. The bones and joints of the hand can be seen in figure 4.7.

4.2.3.1 Bones

The bones that form the wrist and hand are the carpals, metacarpals and phalanges.

The carpals are small, short bones that form the wrist. They are arranged roughly in two rows (a proximal row and a distal row) of four bones each. These small bones allow for the multiple movements possible at the wrist.

The bones in the palm of the hand are called metacarpals. Five metacarpal bones articulate with the distal carpal bones and support the palm.

The bones of the digits are the phalanges. There are three phalanges in each of the second through fifth fingers and two phalanges only in the thumb, also known as the pollex, for a total of 14 phalanges per hand. The proximal phalanx articulates with the head of a metacarpal, while the distal phalanx is the bone in the very tip of the finger. The middle phalanx of each finger lies between the proximal and distal phalanges. [18]

4.2.3.2 Joints

The joints of the hand and wrist are named for the bones which they connect. Each finger has two interphalangeal joints (IPs): distal (DIP) and proximal (PIP). The thumb has only one IP joint. Between the proximal phalanges and the metacarpals are the knuckles or metacarpophalangeal (MCP) joints.

- The MCP are condyloid joints. They allow 0-40 degrees of extension and 85-100 degrees of flexion (figure 4.14a).
- The PIP are ginglymus joints. Their range is from full extension to 90-120 degrees of flexion (figure 4.14b).
- The DIP are also ginglymus joints. Their range is from full extension to 80-90 degrees of flexion (figure 4.14c).
- The thumb MCP is a ginglymus joint and its range goes from full extension to 40-90 degrees of flexion (figure 4.14d).
- The thumb IP is a ginglymus joint and reaches up to 80-90 degrees of flexion (figure 4.14e).

- The CMC joint of the thumb is a unique saddle-type joint. It reaches up to 50-70 degrees of abduction, flexes to a maximum of 15-45 degrees and extends to a maximum of 20 degrees (figure 4.14f). [22]

4.2.4 Phantom limb pain

The amputation of a limb is commonly followed by the sensation that the deafferented (no longer with afferent nerve impulses) body part is still present. These non-painful phantom sensations may include a specific position, shape, or movement of the phantom, feelings of warmth or cold, itching, tingling, or electric sensations and other paraesthesias. Pain in the body part that is no longer present occurs in 50-80% of all amputees. [23]

Phantom limb pain occurs soon after amputation and can be long-lasting. Pre-amputation pain is a risk factor in the development of phantom pain following amputation. Even pain that had been experienced in the limb months or years before amputation can be re-experienced as phantom pain. [24]

Patients may report that the phantom limb is in an awkward position, or that it feels as if it were moving either spontaneously or voluntarily. The phantom limb may feel so real that an amputee may attempt to reach for objects with the phantom hand or try to step with the phantom foot. In addition, most amputees experience a sense of the length and volume of the missing limb.

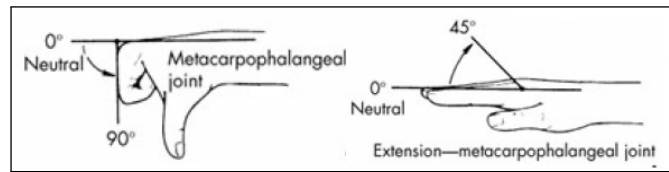
The phantom limb may develop a phenomenon called telescoping. This is most often seen in those with painless phantom limbs, and usually occurs within the first year after amputation. As telescoping occurs, the middle portion of the phantom limb is perceived to be shortened while the most highly innervated area, such as a hand or foot, feels as though it is attached close to or directly on the stump. [24]

The treatments for phantom limb pain are diverse: pharmacological, surgical, anaesthetic, psychological...

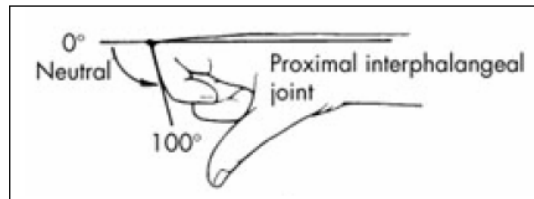
This thesis deals with a behavioural oriented approach, in a similar fashion as the study from Ramachandran and Rogers-Ramachandran in 1996 [25], which was already mentioned in the introductory chapter of this thesis: the mirror box.

Some patients experience involuntary movements in their phantom: such as a clenching spasm of the hand. Voluntary “unclenching” is often effective in relieving the spasm but the patients usually find this very difficult to do because they have no voluntary control over the phantom.

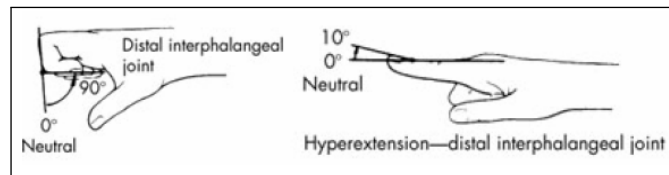
Although the hand is missing, control messages continue to be sent to the muscles in the hand. After all, the part of the brain that controls movements does not ‘know’ that the hand is missing. After a surgical amputation the subject receives no feedback confirming



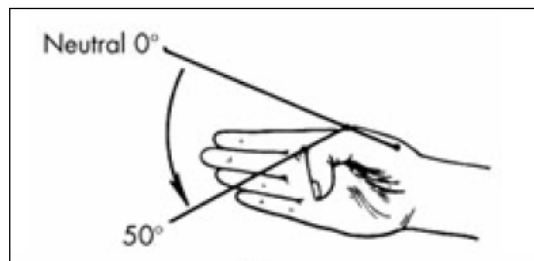
(a) MCP joint: flexion and extension



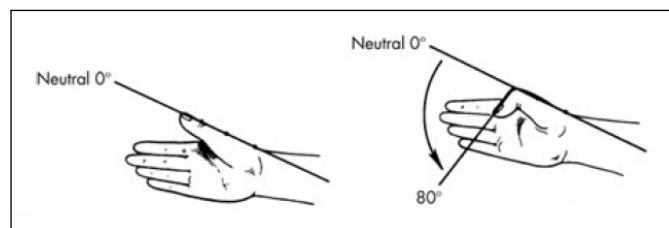
(b) PIP joint: flexion



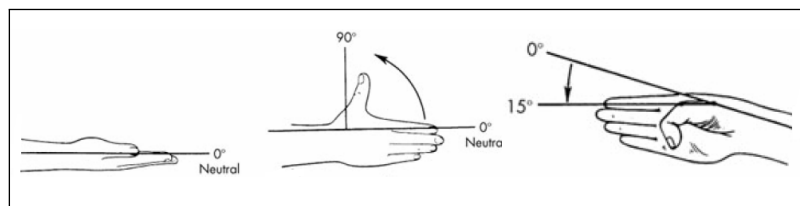
(c) DIP joint: flexion and extension



(d) Thumb MCP joint: flexion and extension



(e) Thumb IP joint: flexion and extension



(f) Thumb CMC joint: abduction and extension

Figure 4.14: Hand joint movements [22]

that the command has been obeyed. Therefore, immediately after amputation the subject can still generate movements in the phantom but with the passage of time this ability is lost because of the prolonged absence of confirming sensory feedback. If this hypothesis of learned paralysis is correct, would it be possible to unlearn the phantom paralysis? To do this, every time the patient sends a message to the phantom arm, he would need to receive a feedback message that his hand is indeed moving correctly. [25]

The mirror box therapy is based on visual feedback. A mirror was placed in a box, and the patient inserted his or her intact arm and the residual limb. He or she was then asked to look at the mirror image of the intact arm, which is perceived as an intact hand where the phantom used to be, and to make symmetrical movements with both hands, thus suggesting real movement from the lost arm to the brain. This procedure seems to re-establish control over the phantom limb and to alleviate pain in some patients. [23]

Phantom limb syndrome is a very old clinical entity that has continued to gain a lot of attention by the medical community and researchers over the past decades. Despite major advances in the understanding of this mysterious phenomenon, a great deal remains to be clarified in terms of both the pathogenesis and treatment of phantom limb syndrome. This thesis presents a non-invasive treatment that, based on the same ideas presented in [25], could help alleviate phantom limb pain.

4.3 Machine Learning

Machine learning studies the design of algorithms able to induce patterns, regularities or rules based on raw data that has been fed into it. Two of the most important machine learning algorithms are supervised learning and unsupervised learning.

Supervised learning generates a function that maps inputs to desired outputs. Basically there is an input, X , an output, Y , and the task is to learn the mapping from the input to the output. On the other hand, the goal of unsupervised learning is to understand the relationships between data components.

The problem of determining the position of the fingers based on features extracted from US images requires clearly a supervised learning approach. The supervised learning algorithm selected to solve the problem is called linear regression.

4.3.1 Regression Analysis

The goal of regression is to predict the value of one or more continuous target variables \mathbf{y} given the value of a N -dimensional vector \mathbf{x} of input variables.

The simplest linear model for regression is one that involves a linear combination of the input variables

$$y_p(\mathbf{x}, \mathbf{w}) = w_0 + w_1x_1 + \dots + w_Nx_N \quad (4.6)$$

where $\mathbf{x} = (x_1, \dots, x_N)^T$, $\mathbf{w} = (w_0, \dots, w_N)^T$. The vector \mathbf{w} is normally called the weights vector and y_p the prediction or guessed output. This is often simply known as *multivariate linear regression* [26]. The key property of this model is that it is a linear function of the parameters w_0, \dots, w_N . It is also, however, a linear function of the input variables x_i , and this imposes significant limitations on the model. For generalization purposes the class of models is extended by considering linear combinations of fixed nonlinear functions of the input variables, of the form

$$y_p(\mathbf{x}, \mathbf{w}) = w_0 + \sum_{j=1}^N w_j \phi_j(\mathbf{x}) \quad (4.7)$$

where $\phi_j(\mathbf{x})$ are known as *basis functions*. By denoting the maximum value of the index j by N , the total number of parameters in this model will be $[N + 1]$. The parameter w_0 allows for any fixed offset in the data and is sometimes called a *bias* parameter. It is often convenient to define an additional dummy ‘basis function’ $\phi_0(\mathbf{x}) = 1$ so that

$$y_p(\mathbf{x}, \mathbf{w}) = \sum_{j=0}^N w_j \phi_j(\mathbf{x}) = \mathbf{w}^T \boldsymbol{\phi}(\mathbf{x}) \quad (4.8)$$

where $\mathbf{w} = (w_0, \dots, w_N)^T$ and $\boldsymbol{\phi} = (\phi_0, \dots, \phi_N)^T$

By using nonlinear basis functions, the function $y_p(\mathbf{x}, \mathbf{w})$ is allowed to be a nonlinear function of the input vector \mathbf{x} . It is common to find in the literature the linear regression explanations with this generalization. Nonetheless, in the work at hand the output y is a linear function of the input \mathbf{x} (features extracted from US images) and the vector $\boldsymbol{\phi}(\mathbf{x})$ of basis functions is simply the identity $\boldsymbol{\phi}(\mathbf{x}) = \mathbf{x}$. Functions of the form (4.7) are called linear models, however, because this function is linear in \mathbf{w} .

Considering now a data set of inputs $\mathbf{X} = \{\mathbf{x}_1, \dots, \mathbf{x}_M\}$ and their corresponding target values $\mathbf{y} = (y_1, \dots, y_M)$. It is then possible to define a $[M, N + 1]$ particular matrix $\boldsymbol{\Phi}$ called *design matrix*

$$\mathbf{\Phi} = \begin{bmatrix} \phi_0(\mathbf{x}_1) & \phi_1(\mathbf{x}_1) & \cdots & \phi_N(\mathbf{x}_1) \\ \phi_0(\mathbf{x}_2) & \phi_1(\mathbf{x}_2) & \cdots & \phi_N(\mathbf{x}_2) \\ \vdots & \vdots & \ddots & \vdots \\ \phi_0(\mathbf{x}_M) & \phi_1(\mathbf{x}_M) & \cdots & \phi_N(\mathbf{x}_M) \end{bmatrix}$$

This matrix can be used to solve equation 4.8 (see, for example, [27])

$$\mathbf{w} = (\mathbf{\Phi}^T \mathbf{\Phi})^{-1} \mathbf{\Phi}^T \mathbf{y} \quad (4.9)$$

This equation can be conveniently decomposed in terms of a $[N+1, N+1]$ matrix $\mathbf{A} = \mathbf{\Phi}^T \mathbf{\Phi}$ and a $[N+1]$ dimensional vector $\mathbf{b} = \mathbf{\Phi}^T \mathbf{y}$ [28]

$$\mathbf{w} = (\mathbf{\Phi}^T \mathbf{\Phi})^{-1} \mathbf{\Phi}^T \mathbf{y} = \mathbf{A}^{-1} \mathbf{b} \quad (4.10)$$

Arrival of a new sample (x_t, y_t) at time step t can thus be described as

$$\mathbf{\Phi}_t = \begin{bmatrix} \mathbf{\Phi}_{t-1} \\ \phi_t \end{bmatrix} \quad \mathbf{y}_t = \begin{bmatrix} \mathbf{y}_{t-1} \\ y_t \end{bmatrix}$$

Integrating these update rules, the matrix \mathbf{A} in equation 4.10 can be formulated recursively as

$$\begin{aligned} \mathbf{A}_t &= \mathbf{\Phi}_t^T \mathbf{\Phi}_t \\ &= \mathbf{\Phi}_{t-1}^T \mathbf{\Phi}_{t-1} + \phi_t^T \phi_t \\ &= \mathbf{A}_{t-1} + \phi_t^T \phi_t \end{aligned}$$

from which we can conclude that each additional training sample constitutes a rank-1 update. Similarly, the update of vector \mathbf{b} can be described recursively as

$$\begin{aligned} \mathbf{b}_t &= \mathbf{\Phi}_t^T \mathbf{y}_t \\ &= \mathbf{\Phi}_{t-1}^T \mathbf{y}_{t-1} + \phi_t^T y_t \\ &= \mathbf{b}_{t-1} + \phi_t^T y_t \end{aligned}$$

Due to these recursive update rules it is *no longer necessary to store previous samples in memory*, instead only \mathbf{A}_t and \mathbf{b}_t are required at each time step. However, the above formulation requires an explicit inversion of \mathbf{A}_t at each update, causing the time complexity to be in $\mathcal{O}((N+1)^3)$. This time complexity can be reduced by directly updating the inverse

of \mathbf{A} , which is known as *Recursive Least Squares* in the field of signal processing. A straightforward method to perform a rank-1 update of the inverse of a matrix is the *Sherman-Morrison formula*

$$\begin{aligned}\mathbf{A}_t^{-1} &= (\mathbf{I} + \Phi_t^T \Phi_t)^{-1} \\ &= (\mathbf{A}_{t-1} + \phi_t^T \phi_t)^{-1} \\ &= \mathbf{A}_{t-1}^{-1} - \frac{\mathbf{A}_{t-1}^{-1} \phi_t \phi_t^T \mathbf{A}_{t-1}^{-1}}{1 + \phi_t^T \mathbf{A}_{t-1}^{-1} \phi_t}\end{aligned}$$

Updating the inverse of the matrix \mathbf{A} reduces the time complexity of adding a sample to an existing model to $\mathcal{O}((N+1)^2)$ and only requires the $[N+1, N+1]$ matrix \mathbf{A}_t^{-1} and the $[N+1]$ dimensional vector \mathbf{b}_t to be stored in memory. The recursion is complete by setting the initial configuration $\mathbf{A}_0^{-1} = \mathbf{I}$ and $\mathbf{b}_0 = 0$. [28]

The simplicity and recursive nature of this update procedure has made it very popular for many applications. In the particular case of this thesis the recursive least squares approach allows the production of a new regression matrix every time an input-output pair is received during the training phase. *Regression matrix* is the term used to describe the group of the six weight-vectors, one for every degree of freedom to be predicted. Thanks to this, it is possible to jump from the training phase to the prediction phase at any time and immediately. Also during the training phase, if the performance of the system goes down, it is possible to jump at once to the training phase, add more data to the system (and *modify* the existing regression matrix) and go back to the prediction phase.

4.4 Image processing

By using image processing techniques information can be easily extracted from photographs or video frames. In this section the basic concepts about digital images are introduced. In addition to that, two important concepts that will be later used in this work are explained: first order surfaces and optical flow.

4.4.1 Digital image

An image is a 2D array of values representing light intensity. For the purposes of image processing, the term image refers to a digital image.

An image is a function of the light intensity

$$f(x, y)$$

where f is the brightness of the point (x, y) and x and y represent the spatial coordinates of a picture element or pixel.

In digital image processing, an imaging sensor converts an image into a discrete number of pixels. The imaging sensor assigns to each pixel a numeric location and a gray level or color value that specifies the brightness or color of the pixel. [29]

4.4.1.1 Image definition

The definition of an image indicates the number of shades that you can see in the image. The bit depth of an image is the number of bits used to encode the value of a pixel. For a given bit depth of n , the image has an image definition of 2^n , meaning a pixel can have 2^n different values. For example, if n equals 8 bits, a pixel can have 256 different values ranging from 0 to 255. If n equals 16 bits, a pixel can have 65,536 different values ranging from 0 to 65,535 or from -32,768 to 32,767. [29]

4.4.1.2 Number of planes

The number of planes in an image corresponds to the number of arrays of pixels that compose the image. A grayscale or pseudo-color image is composed of one plane, while a true-color image is composed of three planes: red component, blue component and green component. In true-color images the color component intensities of a pixel are coded into three different values. A color image is the combination of three arrays of pixels corresponding to the red, green, and blue components in an RGB image. HSL images are defined by their hue, saturation, and luminance values. [29]

4.4.1.3 Conversion from color to grayscale

To convert a RGB image to grayscale the following three algorithms can be applied:

- The **lightness** method averages the most prominent and least prominent colors

$$\text{grayscale value} = \frac{\max(R, G, B) + \min(R, G, B)}{2} \quad (4.11)$$

- The **average** method simply averages the values

$$\text{grayscale value} = \frac{R + G + B}{3} \quad (4.12)$$

- The **luminosity** method is a more sophisticated version of the average method. It also averages the values, but it forms a weighted average to account for human per-

ception. Human eyes more sensitive to green than other colors, so green is weighted most heavily.

$$\text{grayscale value} = 0.2989R + 0.5870G + 0.1140B \quad (4.13)$$

4.4.2 First order surfaces

To extract some characteristic values from the images a definite grid of circles will be deployed over them. From each circle some values will be extracted. These values are called *features* throughout the thesis. The question that remains is: what values to use and how to extract them?

The approach chosen extracts the gray value moments for each sample point in a circular area. To do so a first degree surface is fit to each region of interest by means of a least squares algorithm. A first order surface is described by the following formula

$$Image'(r, c) = \text{Alpha} (r - r_{center}) + \text{Beta} (c - c_{center}) + \text{Gamma} \quad (4.14)$$

where r_{center} and c_{center} are the center coordinates of intersection of the feature region with the full image, *Alpha* denotes the gradient along row direction, *Beta* the gradient along column direction and *Gamma* the offset. [30]

4.4.3 Optical flow

Optical flow is an approximation of the local image motion based upon local derivatives in a given sequence of images. That is, in 2D it specifies how much each image pixel moves between adjacent images while in 3D it specifies how much each volume voxel moves between adjacent volumes. The movement in the images can be caused by objects that move in the world or by a movement of the camera (or both) between the acquisition of the two images.

In both cases, the moving patterns cause temporal varieties of the image brightness. It is assumed that all temporal intensity changes are due to motion only. [31]

4.5 Analysis of results

In order to process the data from the experiments and give an estimation of how good the results are a certain number of parameters will be computed.

4.5.1 Mean

The arithmetic mean is the standard average.

$$\bar{x} = \frac{1}{n} \sum_{i=1}^n x_i \quad (4.15)$$

4.5.2 Standard deviation

In statistics and probability theory, standard deviation (σ) shows how much variation or dispersion exists from the average (mean, or expected value). A low standard deviation indicates that the data points tend to be very close to the mean, whereas high standard deviation indicates that the data points are spread out over a large range of values.

The most commonly used estimator for σ is the *sample standard deviation*

$$\sigma = \left(\sqrt{\frac{1}{n-1} \sum_{i=1}^n (x_i - \bar{x})^2} \right) \quad (4.16)$$

where $\{x_1, x_2, \dots, x_n\}$ are the observed values of the sample items and \bar{x} is the mean value of these observations.

4.5.3 Mean Absolute Error

In statistics, the mean absolute error (MAE) is a quantity used to measure how close predictions are to the eventual outcomes. The mean absolute error is given by

$$MAE = \frac{1}{n} \sum_{i=1}^n |p_i - y_i| = \frac{1}{n} \sum_{i=1}^n e_i \quad (4.17)$$

where p_i is the prediction and y_i is the true value.

4.5.4 Normalized Root Mean Squared Error

The Root Mean Squared Error (RMSE) is a measure of the differences between values predicted by a model or an estimator and the values actually observed

$$RMSE = \sqrt{\frac{\sum_{i=1}^n (p_i - y_i)^2}{n}} \quad (4.18)$$

where p_i is the prediction and y_i is the true value. Expressing the formula in words,

the difference between prediction and corresponding observed values are each squared and then averaged over the sample. Finally, the square root of the average is taken. Since the errors are squared before they are averaged, the RMSE gives a relatively high weight to large errors. This means the RMSE is most useful when large errors are particularly undesirable.

The Normalized Root Mean Squared Error (NRMSE) is the RMSE divided by the range of observed values

$$NRMSE = \frac{RMSE}{y_{max} - y_{min}} \quad (4.19)$$

The value is often expressed as a percentage where lower values indicate less residual variance.

4.5.5 Correlation Coefficient

The correlation coefficient (r or ρ or CC) measures the strength and the direction of a linear relationship between two variables. It gives an idea of the quality of a least squares fitting to the original data.

The correlation coefficient is a number between -1 and 1. A CC value of -1 indicates a perfect negative fit. Negative values indicate a relationship between x and y such that as values for x increase, values for y decrease. If there is no relationship between the predicted values and the actual values the correlation coefficient is 0 or very low. Finally a correlation of +1 indicates a perfect positive fit. Positive values indicate a relationship between x and y such that as values for x increase, values for y also increase.

The CC can be computed with the following formula

$$r_{xy} = \frac{n \sum x_i y_i - \sum x_i \sum y_i}{\sqrt{n \sum x_i^2 - (\sum x_i)^2} \sqrt{n \sum y_i^2 - (\sum y_i)^2}} \quad (4.20)$$

where n is the number of observations.

5

Hardware

This project involves the integration of several hardware devices into a single PC application. The general scheme of the setup is displayed in figure [5.1](#).

5.1 Ultrasound portable system

The ultrasound system used in this project is the model LOGIQe from General Electric Healthcare. The LOGIQe system is a portable ultrasound machine of the size of a notebook and is displayed in figure [5.2](#). This model is designed for cardiac, abdominal, obstetrics, gynecology, vascular, musculoskeletal, small parts, pediatric, neonatal and intraoperative applications.

The probe that will be used with the system is the model GE 12L-RS, also from General Electric Healthcare. The GE 12L-RS is a linear array probe that operates with a frequency between 5 and 13 MHz.

Following an empirical procedure the optimal configuration of the system was determined and is displayed in table [5.1](#). The objective of this configuration is to obtain ultrasound images as different as possible when performing the different finger movements.

Parameter	Explanation	Setting
Mode	Choose between M-Mode, B-Mode, Colour Flow Mode and Doppler Mode	B-Mode
Transducer Frequency	Adjust transducer's frequency	12.0 MHz
Gain	Control the amount of echo information displayed in an image	18
Edge Enhancement	Brings out subtle tissue differences and boundaries by enhancing the gray scale differences corresponding to the edges of structures	5/4
Number of focus zones	Focal zone to tighten up the beam for specific areas	2
Map	Determines how the echo intensity levels received are presented as shades of gray	J/0
Depth	The field of view	4 cm
Dynamic Range	Controls how echo intensities are converted to shades of gray, thereby increasing the adjustable range of contrast	93
Rejection	Selects a level below which echoes will not be amplified	0
Auto Optimise	Optimise the image based upon a specified region of interest	100%
Time Gain Compensation	Amplifies the returning signals to correct the attenuation caused by tissues at increasing depth	low
Frame Rate	Resulting frame rate	20 Hz

Table 5.1: Optimized parameters for the ultrasound system [32] & [14]

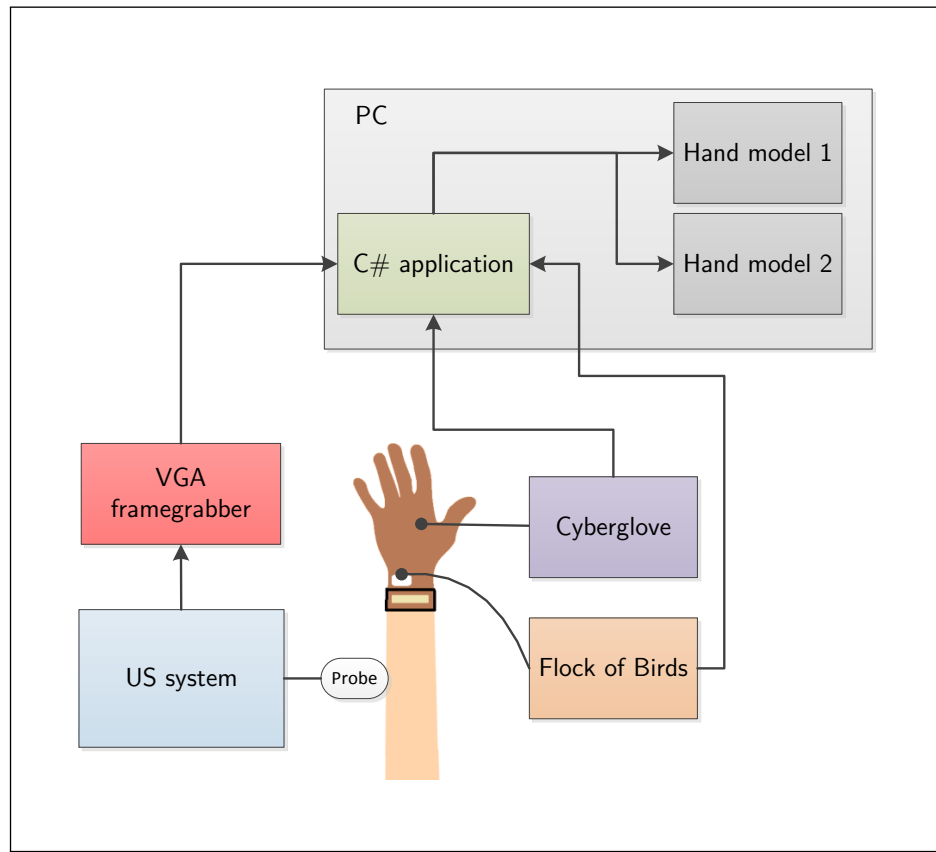


Figure 5.1: General scheme of the setup

5.2 Cyberglove

The CyberGlove from *CyberGlove Systems* is a fully instrumented glove that provides up to 18 high-accuracy joint-angle measurements. It uses proprietary resistive bend-sensing technology to accurately transform hand and finger motions into real-time digital joint-angle data.

The use of the Cyberglove in the project provides an accurate measure of the positions of the fingers, which will help greatly during the development phases, especially when it comes to analyzing the errors in the prediction.

The model used in this project features two bend sensors on each finger, four abduction sensors, plus sensors measuring thumb crossover, palm arch, wrist flexion and wrist abduction. The producer guarantees a resolution of 0.5 degrees, a repeatability of 1 degree and a maximum nonlinearity of 0.6% over the full joint range. The interface is RS-232 with maximum transfer rate of 115.2 kbaud.



Figure 5.2: Ultrasound system LOGIQe (General Electric)

5.3 Framegrabber

The Epiphan VGA2Ethernet is a compact external network framegrabber that is capable of capturing single link DVI, HDMI1 and VGA signals at rates of up to 60 frames per second. VGA2Ethernet also supports a stereo 3.5mm audio input. Epiphan Systems VGA2Ethernet uses a common RJ45 10/100/GigE Ethernet port to interface itself with the target computer, allowing for up to 1 Gigabit transfer rates. [33]

The need of this device in the project stems from the fact that the ultrasound system LOGIQe does not have an interface to stream the images directly to the computer. A library is included with the software and can be accessed from the C# application.

This device includes hardware compression making the maximum real frame rate also depend on the entropy of the input VGA signal. In other words, the frame rate depends on how well the signal can be compressed and on how different a frame is from the previous one.



Figure 5.3: Cyberglove (CyberGlove Systems)



Figure 5.4: VGA to Ethernet Framegrabber (Epiphan systems Inc.)

5.4 Flock of birds

The Flock of Birds is a magnetic tracker developed by Ascension Technology Corp. The function of this device in the project will be to track the changes in the angle of the wrist during the experiments.

Some relevant characteristics of this device are detailed in table [5.2](#).

Parameter	Value
Tracking range	$\pm 30^\circ$ (.75m) accuracy
Angular range	$\pm 180^\circ$ Azimuth & Roll, $\pm 90^\circ$ Elevation
Static position accuracy	1.8 mm RMS
Orientation	0.5° RMS
Static position resolution	0.5mm @ 30.5cm
Orientation	0.1° @ 30.5cm
Update rate	Up to 144 measurements/second
Outputs	X, Y, Z positional coordinates and orientation angles, or rotation matrix
Interface	RS-232 with selectable baud rates up to 115200
Format	Binary
Modes	Point or Stream

Table 5.2: Characteristics of the Flock of Birds [34]



Figure 5.5: Flock of birds (Ascension Technology Corporation)

5.5 Probe holder

When this project started one year ago the probe of the ultrasound system was held and pressed against the arm during the experiments by a drill holder. Last year, when

an amputee visited the DLR's Institute in Oberpfaffenhofen to test the feasibility of the project, it became clear that a new probe holder was needed. The amputee was not comfortable with the drill holder and the experiments had to be done with an improvised setup, which had a very negative impact on the results.

The design engineer Tilo Wüsthoff came up at the beginning of 2012 with a device that successfully attaches the transducer of the ultrasound system to the arm. The 3D model of this device is shown in figure 5.6. The device disassembled and attached to the arm can be seen in figure 5.7.

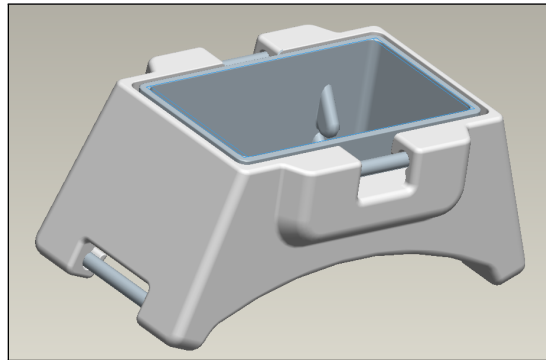
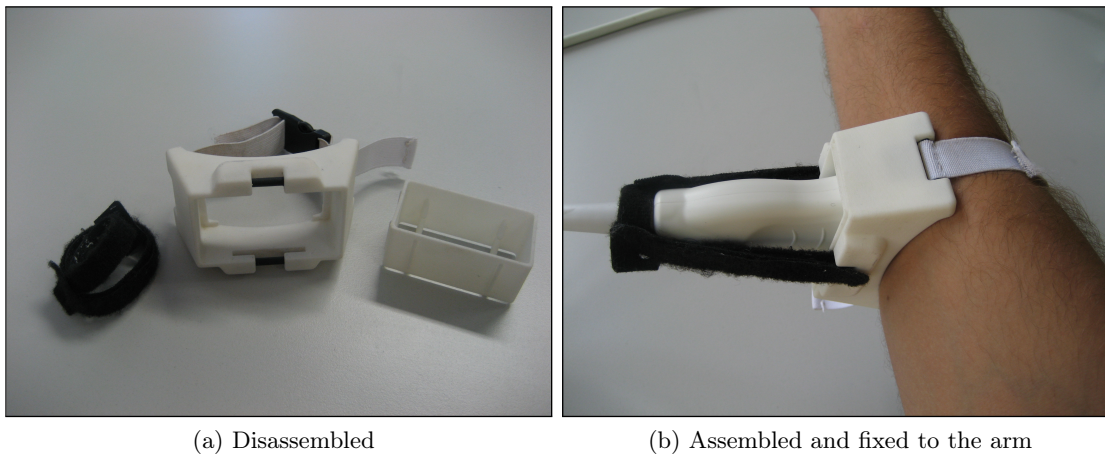


Figure 5.6: PRO/Engineering model of the probe holder



(a) Disassembled

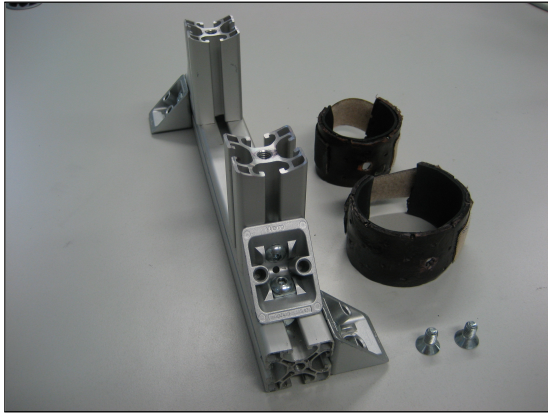
(b) Assembled and fixed to the arm

Figure 5.7: Arm adjustable probe holder

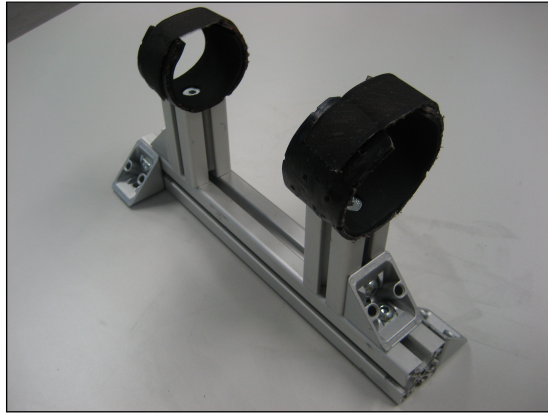
However, this fixation could not be used with the arm laying on the table, as it was custom. A new setup was developed to be used in conjunction with Tilo's holder. The objective was to leave the whole circumference of the forearm free, in order to be able to explore all possible positions with the US probe in search of the best quality of the features. Also, the new setup was expected to be flexible in order to be adaptable for amputees.

With these two targets in mind a simple structure was constructed and is displayed in figures 5.8a and 5.8b. The arm bands consist of a thermoplastic material and were molded

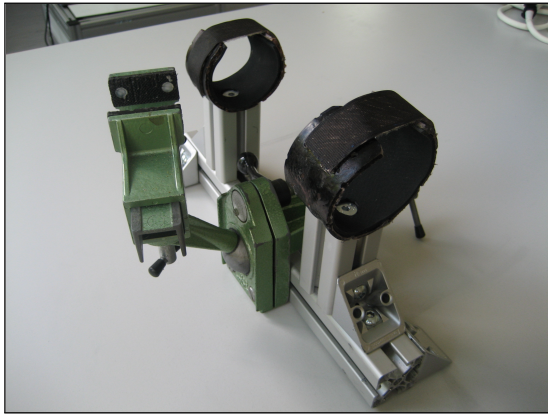
with the shape of the forearm. The interior of the arm bands is made of rubber so that they do not hurt the patient. The structure itself is constructed using Item profiles, which gives the setup a high versatility.



(a) Disassembled



(b) Assembled



(c) Assembled and with the drill holder extension



(d) Whole setup

Figure 5.8: Evolution of the probe holder

During the experiments it was detected that the new holder would slide over the arm, mostly due to the presence of gel between the transducer and the skin. A drill holder was finally attached to the structure, keeping the probe definitely fixed during the whole duration of the experiments.

6

Software

6.1 Visual Studio C#

C# is a simple, modern, general-purpose, object-oriented programming language. It has a very clear syntax and allows fast developing times thanks to its low learning curve. A large part of the power of C# (as with other .NET languages), comes with the common .NET Framework API, which provides a large set of classes, including ones for encryption, TCP/IP socket programming, and graphics.

Microsoft Visual Studio is an integrated development environment (IDE) from Microsoft. It is used to develop console and graphical user interface applications along with Windows Forms applications, web sites, web applications, and web services in both native code together with managed code for all platforms supported by Microsoft Windows, Windows Mobile, Windows CE, .NET Framework, .NET Compact Framework and Microsoft Silverlight.

Visual Studio supports different programming languages by means of language services, which allow the code editor and debugger to support (to varying degrees) nearly any programming language, provided a language-specific service exists. Built-in languages include C/C++, VB.NET, C# and F# (as of Visual Studio 2010). Support for other languages such as M, Python, and Ruby among others is available via language services installed separately.

6.2 MVTec's Halcon

HALCON is a comprehensive standard software for machine vision with an integrated development environment that is used worldwide. It enables cost savings and improved time to market: HALCON's flexible architecture facilitates rapid development of machine vision, medical imaging and image analysis applications.

HALCON provides outstanding performance and a comprehensive support of multi-core platforms, SSE2 and AVX, as well as GPU acceleration. It serves all industries with a library of more than 1800 operators for blob analysis, morphology, matching, measuring, identification and 3D vision. [35]

HALCON offers a native .NET interface providing access to a wide range of operators and functions.

The IDE offered by HALCON will be exclusively used for rapid tests and theoretical problems. In the final application its functions will be accessed using the .NET interface.

6.2.1 Optical flow in Halcon

The operator *optical_flow_mg* provided by Halcon computes the optical flow between two images.

The two consecutive images of the image sequence are passed in *Image1* and *Image2*. The computed optical flow is returned in *VectorField*. The vectors in this vector field represent the movement in the image plane between *Image1* and *Image2*. The point in *Image2* that corresponds to the point (r, c) in *Image1* is given by

$$(r', c') = (r + u(r, c), c + v(r, c))$$

where $u(r, c)$ and $v(r, c)$ denote the value of the row and column components of the vector field image *VectorField* at the point (r, c) .

Three different algorithms for computing the optical flow can be used. All three algorithms are implemented by using multigrid solvers to ensure an efficient solution of the underlying partial differential equations.

- Algorithm 'fdrig': the method proposed by Brox, Bruhn, Papenberg and Weickert. This approach is flow-driven, robust, isotropic and uses a gradient constancy term.
- Algorithm 'ddraw': a robust variant of the method proposed by Nagel and Enkelmann. This approach is data-driven, robust, anisotropic and uses warping (in contrast to the original approach).

- Algorithm ‘clg’: the combined local-global method proposed by Bruhn, Weickert, Feddern, Kohlberger, and Schnörr. [30]

6.3 MATLAB

MATLAB (matrix laboratory) is a numerical computing environment. Developed by MathWorks, MATLAB allows matrix manipulations, plotting of functions and data, implementation of algorithms, creation of user interfaces, and interfacing with programs written in other languages, including C, C++, Java, and Fortran.

MATLAB will be primarily used to analyze the data obtained from the experiments.

6.4 Numerical library: ALGLIB

ALGLIB is a cross-platform numerical analysis and data processing library. It supports several programming languages (C++, C#, Pascal, VBA) and several operating systems (Windows, Linux, Solaris). ALGLIB features include:

- Linear algebra
- Solvers (linear and nonlinear)
- Interpolation
- Optimization
- Fast Fourier Transforms
- Numerical integration
- Linear and nonlinear least-squares fitting
- Ordinary differential equations
- Statistics (descriptive statistics, hypothesis testing)
- Data analysis (classification/regression, including neural networks)
- Multiple precision versions of linear algebra, interpolation optimization and others algorithms

ALGLIB is open source and can be used for free under GPL 2+. [36]

This library is used in the project to calculate some very basic matrix operations and, over all, compute the Sherman-Morrison formula efficiently.

6.5 Hand Model

A 3D Hand model will be used to display the stimulus and predictions on the screen. This hand model was created in Blender by a student called Uwe Jaschke and can be controlled via UDP.

A string consisting of 22 values needs to be sent via UDP to the Hand model in order to move it. The format of this string is the following:

$$\text{String chain} = [v0, v1, v2, , v19, v20, v21]$$

colons and square brackets inclusive. The meaning of each of these 22 values is detailed below:

- | | |
|--------------------------|---------------------------|
| 1. Thumb CMC1 adduction | 12. Middle DIP3 |
| 2. Thumb CMC1 rotation | 13. Ring MCP4 adduction |
| 3. Thumb MCP | 14. Ring MCP4 |
| 4. Thumb IP1 | 15. Ring PIP4 |
| 5. Index MCP2 adduction | 16. Ring DIP4 |
| 6. Index MCP2 | 17. Pinkie MCP5 adduction |
| 7. Index PIP2 | 18. Pinkie MCP5 |
| 8. Index DIP2 | 19. Pinkie PIP5 |
| 9. Middle MCP3 adduction | 20. Pinkie DIP5 |
| 10. Middle MCP3 | 21. Wrist Flexion |
| 11. Middle PIP3 | 22. Wrist Adduction |

This thesis is focused on predicting the movements of 1, 2, 6, 10, 14 and 18.

System analysis

7.1 Modes of operation

When the system is running the user can see on the screen the graphical user interface and two 3D hand models (figure 8.2). By using the GUI, the different modes of operation can be selected and the course of the experiment controlled. Table 7.1 summarizes the different modes of operation of the system along with the functions of the two hand models.

Method	Operation	Hand model #1	Hand model #2
<i>Cyberglove</i>	Train	Inactive	Stimulus
	Predict	Prediction	Stimulus
<i>Stimulus</i>	Train	Inactive	Stimulus
	Predict	Prediction	Stimulus

Table 7.1: Modes of operation

7.1.1 Method: Cyberglove

The Cyberglove provides exact information about the position of the fingers. This exact information is used first to train the system and, most importantly, to compute the error of the prediction during the predicting phase. That is why the Cyberglove is a vital piece of equipment during the development phase of the project.

- During the **training phase** a stimulus is shown on one of the hand models while the other stays inactive. The user is asked to mimic the movements of the stimulus. In this phase features are extracted from the US images and matched to the position information of the Cyberglove.

Additionally to the hand model of the stimulus it would be possible to display the position feedback given by the Cyberglove on the other hand model . However, as experiments were being conducted, the subjects were clearly more focused on matching the movements of the two hand models than on performing natural and easy to reproduce movements. For this reason only one of the hand models is used at this stage.

- During the **prediction phase** a stimulus is still shown on one of the hand models while on the other the prediction is displayed. The subject is asked to mimic the movements of the stimulus. By showing both of them simultaneously it is easy to spot which finger movements are not performing as expected and need to be retrained.

Optionally the real position of the fingers given by the Cyberglove could be displayed on one of the hand models instead of the stimulus. This would allow to check more dynamically which DoF are working in a satisfactory manner. For the experiments and the analysis of errors the use of the stimulus is however mandatory, for it somehow guarantees that the movement of every finger is done with the same speed and duration. This way the results obtained with different subjects are comparable.

During this phase both the Cyberglove feedback as the prediction are stored. At the end of the experiment all the information is written to the disk and can be processed offline.

7.1.2 Method: Stimulus

This project is intended to be used by amputees and therefore the use of the Cyberglove is restricted only to healthy subjects during the development stages. In the final version a stimulus signal will replace the Cyberglove.

- As in the case of the Cyberglove method, during the **training phase** a stimulus signal is shown on one of the hand models while the other remains inactive. There is however

a big difference and that is that the position information is directly taken from the stimulus, which is considered the *ground truth*. In this phase it is extremely important that the patient replicates with as much precision as possible the movements of the stimulus.

- During the **prediction phase** a stimulus is still shown on one of the hand models while on the other the prediction is displayed. By showing both of them simultaneously it is easy to spot which finger movements are not performing as expected and need to be retrained.

As in the case of the Cyberglove method, the subject is asked to mimic the movements of the stimulus. In this phase it is also vital that the user follows the stimulus as closely as possible. At the end the experiment the position data from the stimulus and from the prediction will be stored to the disk for offline processing. There will be delays between both signals, for it is impossible that the user can follow the prediction with a 1:1 precision. Nonetheless, the delays will have a huge impact on the prediction error and this should be taken into account when analyzing the results.

7.2 Graphical User Interface

It is said an image is worth a thousand words. Analyzing the graphical user interface will serve as an introduction to the workflow of the program and also as a guide to explain some new concepts.

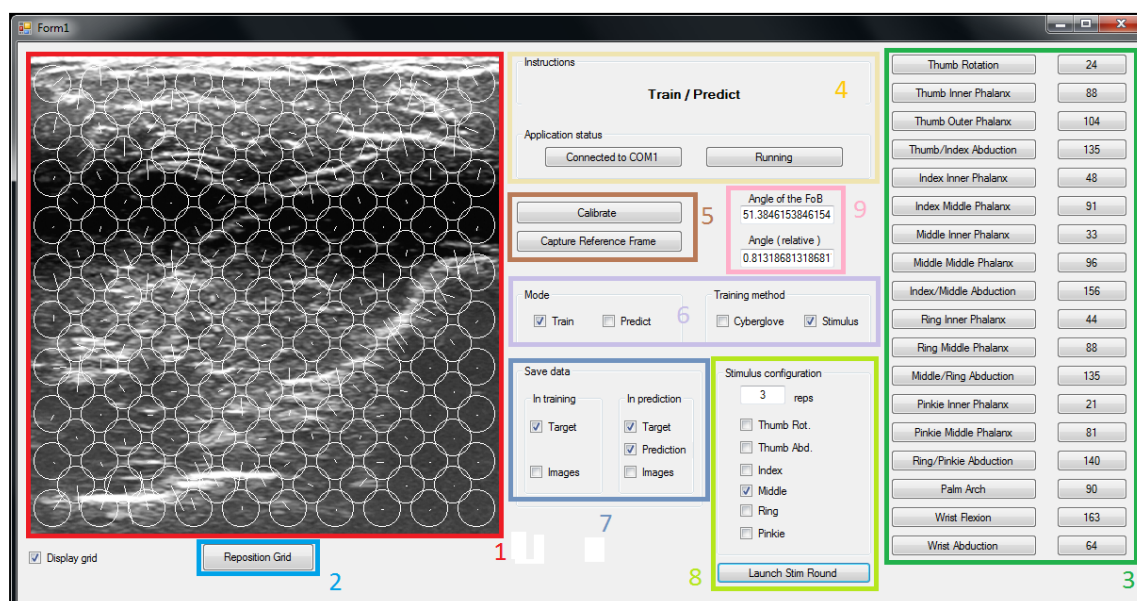


Figure 7.1: Graphical User Interface during an experiment

1. **Display**

The display shows in real time the images from the US unit that are being captured with the VGA framegrabber. In addition to that, and superimposed to the images, the grid of regions of interest from which the features will be extracted is displayed.

For each region of interest (or circle) three numerical values are extracted (Alpha, Beta and Gamma, as explained in section 4.4.2). By using the first two of them, which represent the gray value gradients along row and column direction respectively, a vector is displayed within each region of interest. This vector changes in real time with the images and gives an idea of whether the features are being correctly extracted or not.

The number of feature points as well as the radius of the regions of interest were selected following an empirical process. As much surface of the images as possible needs to be covered by the regions of interest, trying to avoid overlapping and without having too many of them, which would cause a brutal increase of the processing times. The final grid consists of 181 regions of interest with a radius of 20 pixels each, which translates into a total of 543 features extracted from each frame.

2. **Reposition grid**

The reposition grid routine is what remains of the experiments ran without the new physical setup. The probe of the US system would continuously shift over the arm during the experiments, affecting the prediction. If that happened, the user would set the hand in the rest position and click on the reposition grid button. In that instant, the current frame was compared to a reference frame stored at the beginning of the experiment and, by examining the optical flow between the two, the grid would shift trying to adapt to the new position of the probe. There is no longer need for this routine and will not be used during the final experiments.

3. **Cyberglove sensor readings**

The whole set of Cyberglove sensors and their readings ranging from 0 to 255 are displayed on the right side of the GUI.

4. **Information panels**

They provide information about the state of the system and show the instructions that the user must follow during the experiment.

5. **Calibrate Cyberglove**

At the beginning of the experiment the values from the Cyberglove sensors are captured with the fingers in relaxed and flexed position. This permits to have a measure of the degree of change for each angle and obtain the values that need to be sent to the 3D hand models.

Capture reference frame

A US frame from the user in rest position is stored to the disk for information purposes only. The relative angle of the Flock of Birds is then reset. The user will be asked to try to keep it stable during the duration of the experiment.

6. Experiment configuration

These panels allow the user to choose between the Cyberglove or the stimulus training modes, and to switch between the training and prediction phases.

7. Data saving

In this panel it is possible to choose the information that will be written to the disk. Writing data to the disk implies however a lot of time. Therefore the data is stored in dynamic variables that grow in size as the experiment goes by. At the end of the experiment, when the form is closed, all this information is finally saved to the disk.

8. Stimulus configuration

The user can configure the stimulus that will be displayed on the 3D hand model: which degrees of freedom to move and with how many repetitions. The movements always start with the pinkie (if selected) and end on the thumb rotation.

9. Angle of the Flock of Birds

In order for the user to keep the wrist stable during the experiment the angle of pronation/supination of the wrist is displayed in the GUI. The relative angle is set to zero at the beginning of the experiment when the user is in rest position and the reference frame is captured.

The natural flow of an experiment is displayed in figure 7.2. The functions of the two 3D hand models during the training and prediction phases were previously commented in table 7.1.

7.3 Inside the C# application

Figure 5.1 showed the interactions the C# application has with external hardware and other pieces of software. In order to attend all devices a multi-threaded application was implemented with a total of four threads:

- Main thread: configures the program, launches the other threads and updates the GUI.
- *poll_cg*: retrieves continuously data from the Cyberglove.

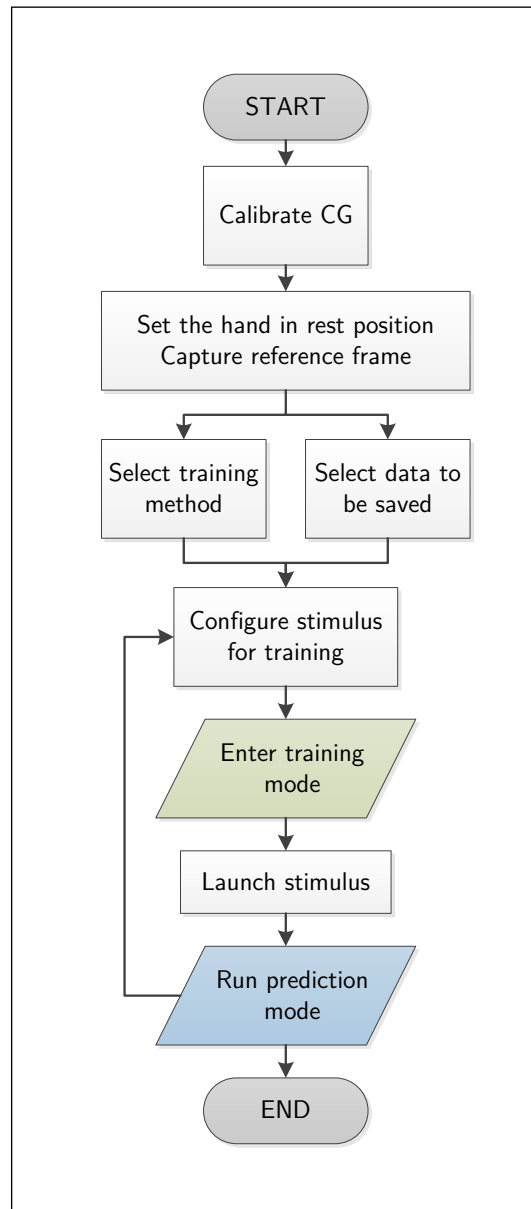


Figure 7.2: Natural flow of an experiment

- *poll_fg*: retrieves continuously frames from the VGA framegrabber. The regression algorithm and therefore the training and prediction are done by this thread.
- *poll_fob*: retrieves continuously information about the angle around the X axis of the Flock of Birds emitter.

The way the threads interact between them and the description of what they do is detailed in this chapter.

7.3.1 Interactions between threads and timing analysis

The different threads running in the application need to share data between them. In order to avoid two threads trying to access simultaneously the same variable (portion of memory) synchronizing objects called *lockers* are used. Only one thread can lock a variable at a time.

The main functions that each thread performs are detailed in the next page.

Both the Cyberglove as the Flock of Birds use RS-232 to communicate with the computer. Since the amount of information that they provide is relatively small in size, the information is updated rather fast, receiving new data on average every 11.4 ms and 2.6 ms, respectively (figure 7.3).

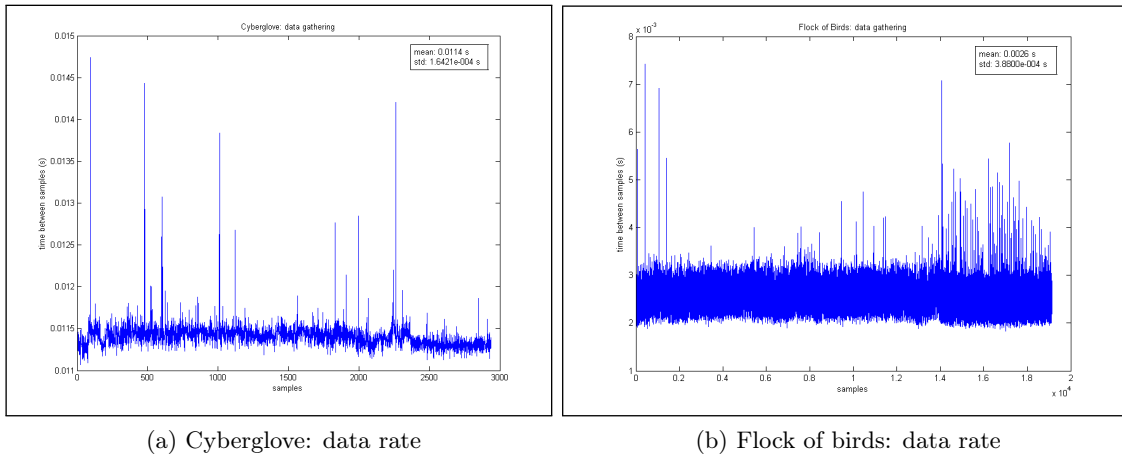


Figure 7.3: Data rates from the Cyberglove and the Flock of Birds

On the other hand, the size of the data that the VGA framegrabber supplies to the system is in comparison quite big, requiring 17.3 ms on average to provide a new frame (figure 7.4).

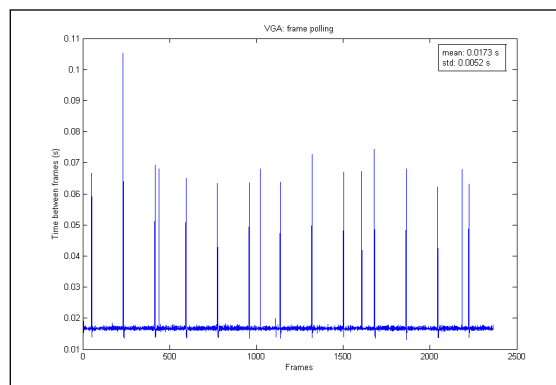


Figure 7.4: Data rate from the framegrabber

MAIN THREAD

- Configures and initializes the system:
variables, GUI, paths of the data, UDP ports
- Initializes serial connection with the Cyberglove
 - Initializes serial connection with the Flock of Birds
- Initializes the Ethernet connection with the VGA framegrabber
 - Launches Cyberglove thread
 - Launches Flock of Birds thread
- Sets up a timer that updates the GUI:
ticks every 20ms (50 Hz)

(Cyberglove configured?)

- Launches Framegrabber thread

Updates GUI

Callbacks

- CG calibration
- Stimulus management
each new stimulus a 10 ms timer is created to create the signal: DataSTIM
- Method of training: CG or stimulus
- Mode: training or predicting
-
- Form closes: save data to the disk

DataCG

AngleFOB

DataSTIM

CYBERGLOVE THREAD

- Requests serial data to the Cyberglove
- Stores data in DataCG

FLOCK OF BIRDS THREAD

- Configures FoB mode (only angles)
- Requests serial data to the FoB
- Stores data in AngleFOB

FRAMEGRABBER THREAD

- Grabs new frame from the framegrabber
 - Captures the last updated
DataCG & AngleFOB & DataSTIM
- Asks *image processing routine* for features data

(last frame ok?)

- Train or predict

Image processing routine

- Compares new frame with the last one
- (Is it not a teared frame?)
- Extracts features

Training

- Uses new features to update Ainv with the Sherman-Morrison formula
- Uses new Ainv and new (DataCG or DataSTIM) to update w (weights matrix)

Predicting

- Uses w and new features to produce the prediction
- Filters the prediction with an average filter to avoid flickering
- Sends the filtered prediction to the Hand Model via UDP

The VGA framegrabber is providing then frames every 17.3 ms. However, in the configuration parameters of the ultrasound system in section 5.1 the refresh frequency is 20 Hz, that is, 50 ms. How is this possible?

The VGA framegrabber is not synchronized with the US system and this is a big problem. Before the whole frame in the US system is completely refreshed the VGA captures it and feeds it into the system. The result of this is that the system receives *teared frames* that should be filtered out. An example of teared frames is displayed in figure 7.5. Figure 7.5a shows the previous frame and figure 7.5a shows the next frame, in which only the upper part is updated.

A software solution was implemented to detect the teared frames. Using the functions provided by the API of Halcon the absolute difference of every new arriving frame with respect the previous one is calculated, giving as a result a new image. The intensities in the upper and lower part of this new image are compared with a threshold value which was set empirically. If both parts of the image have changed the new frame will be accepted. Otherwise the frame will be considered a teared frame and no features will be extracted from it.

After applying this algorithm the rate of accepted frames changes from the 17.3 ms on average of figure 7.4 to the 52.7 ms on average of figure 7.6.

7.4 Compensation of the pronation wrist

The relative movements of the US probe with respect of the arm of the patient during the experiments were considered the main cause of the decay in the performance of the system overtime. With the new probe holder introduced in section 5.5 this problem has been solved.

However, even with the new probe holder, sudden drops in the quality of the prediction were experienced when running experiments with some test subjects. A new problem was detected. When a patient turns the wrist, even in a very small angle, the US images change radically. This can be seen in figure 7.7.

Because it would be almost an impossible task to implement a physical setup that would keep subjects from performing these small movements of the wrist (and useless when having amputees using the system) a software solution is proposed.

If the angle of the wrist is tracked during the experiment with the Flock of Birds it would be possible to shift the grid of the regions of interest proportionally. To do so, at the beginning of the experiment the subject would be asked to turn the wrist on purpose.

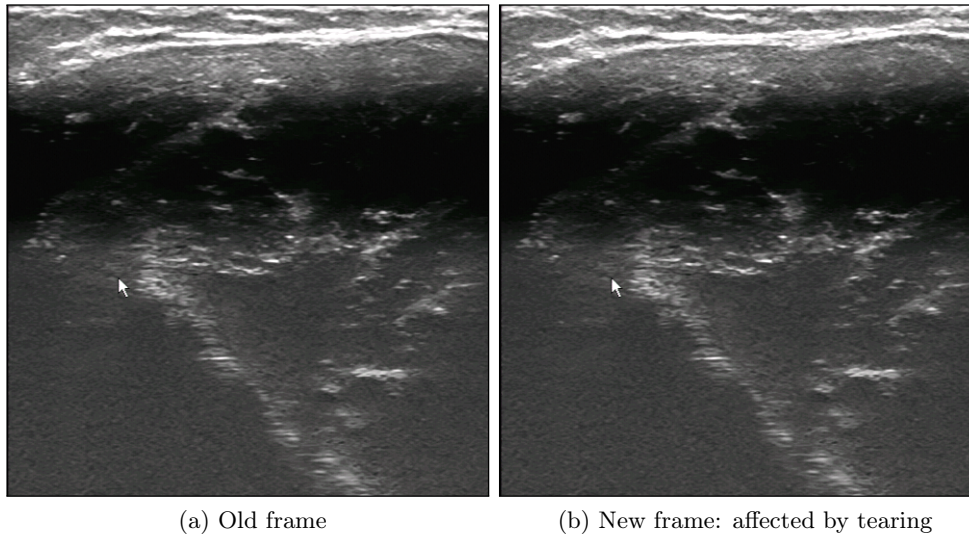


Figure 7.5: Example of teared frame

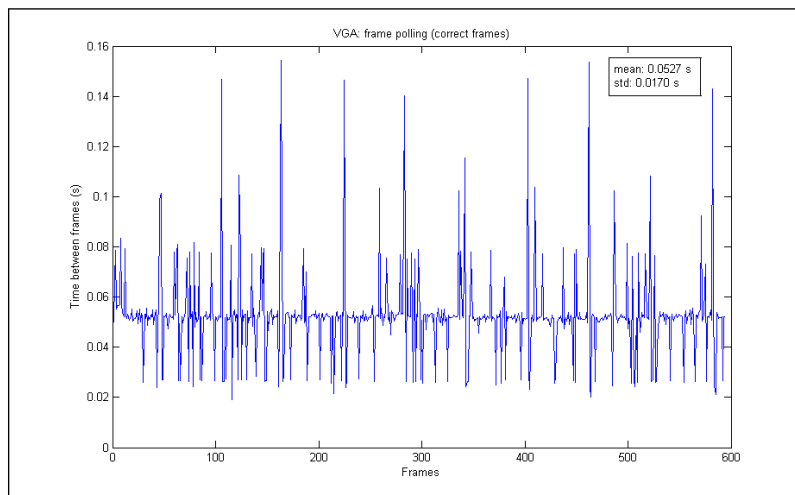


Figure 7.6: Data rate from the framegrabber without teared frames

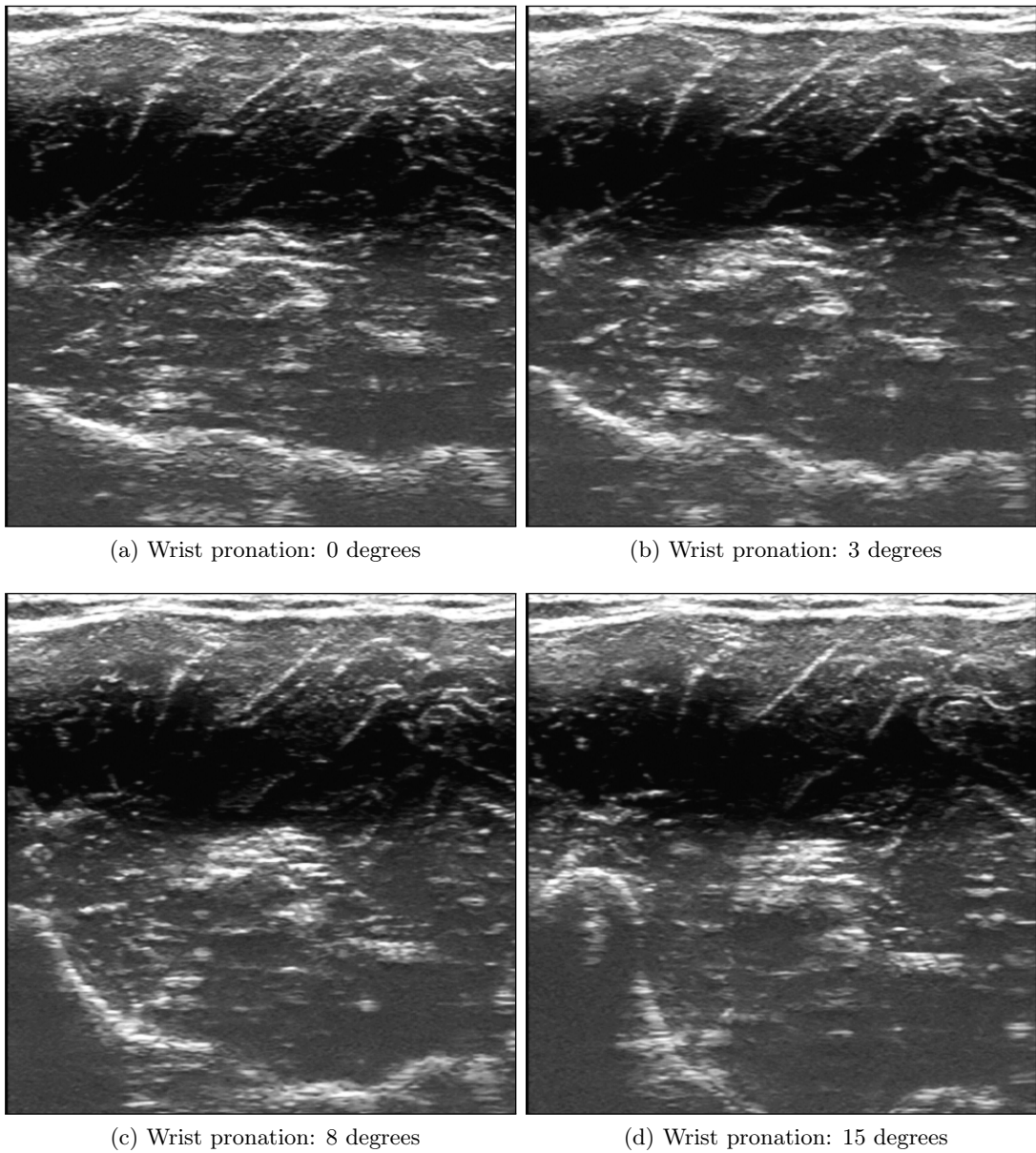


Figure 7.7: Changes in the US images with the wrist angle

During this movement angles and images would be captured simultaneously. By computing these captured frames with optical flow techniques, it is possible to obtain a measure of how much the grid needs to be shifted at every given angle.

This idea has been tested using the Halcon integrated development environment. Optical flow was applied to the four frames displayed in figure 7.7. The result for every computation is a field of vectors that gives information about how each image has changed with respect the previous one. With this information it is plausible to shift the grid of points in charge of extracting the features, in order to somehow “track the features” accordingly with the changes of the images. The results are displayed on figure 7.8

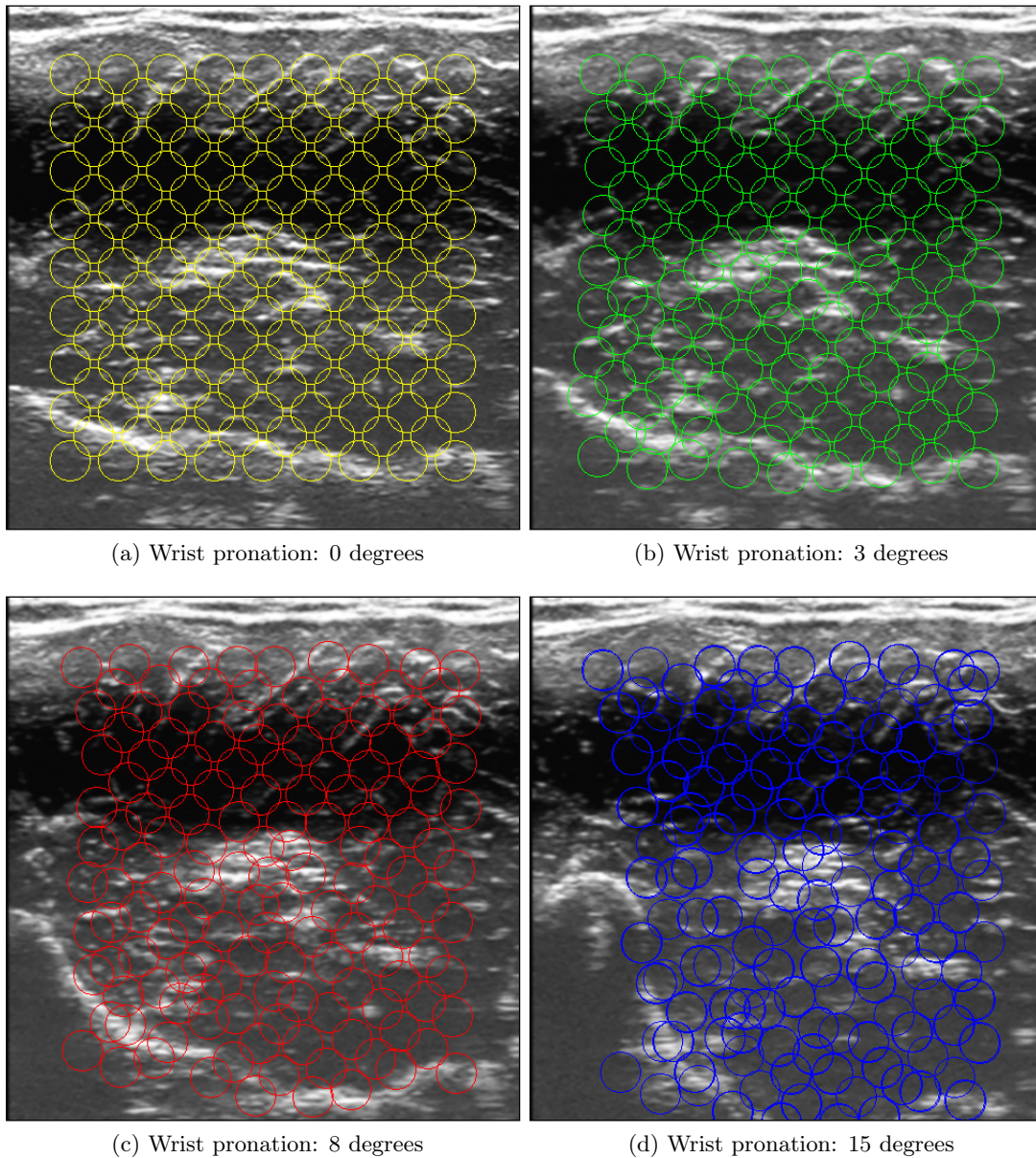


Figure 7.8: Shifting of the regions of interest proportionally to the wrist angle

It is clearly noticeable how some of the regions of interest that in the first frame are located over a bright area shift in the rest of the frames following the bright area.

To give an estimation of how effective this approach could be an analysis of the error was conducted. The known features (alpha, beta, gamma) will be extracted from every frame with the original and the shifted grid and then compared to the perfect case, that is, the values obtained from the static grid on the first image.

The results obtained are displayed in figure 7.9. The adaptive grid reduces the NRMSE by 50% for all three features compared to the initial static grid.

This constitutes a theoretical study on how to tackle the problem of the wrist pronation. Considering the results, this approach should definitely be taken into account in the next iterations of the project.

In the tests conducted in this thesis this technique will not be applied and the Flock of Birds will be used only to display on the GUI the current value of the wrist angle. This will give the subjects a reference to try and keep the wrist stable.

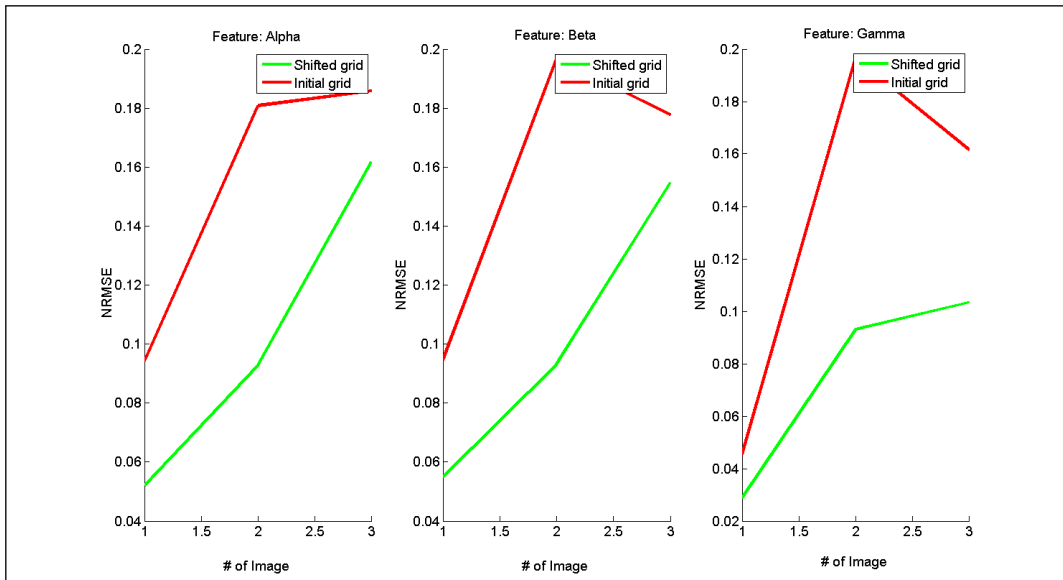


Figure 7.9: Effect of the dynamic grid on the error

8

Experiments

With the objective of producing a reliable measure of how good the performance of the system is, a series of tests will be carried out on a number of subjects. The target of this thesis is to obtain an accurate and reliable prediction and a system dynamic enough to compensate the changes in the conditions of the experiments and therefore capable of running for a relative long time. These experiments pretend to determine if these objectives were met.

8.1 Preliminary experiment

8.1.1 Description

The setup used in older iterations of the project consisted only of a drill holder that would keep the probe in vertical position against the ventral side of the forearm. The new setup is described in section 5.5 and allows to fix the probe in any part of the forearm and to keep it stable during the duration of the experiment.

However, before starting with the main test it is necessary to confirm that the latest physical setup yields indeed better results than the one used in previous works. The sensations when using the latest version of the system with both setups already indicate so but that sensations need to be put into numbers.

With this objective a simple test was conducted under the following conditions:

- Only one degree of freedom is tested: flexion of the middle finger. This has two advantages. First, the time of the experiment can be kept short, while still being able to test the prediction on a high number of movements. Second, the quality of the prediction is normally higher when less degrees of freedom are trained (there are less interactions between the features of the different degrees of freedom). This last condition will reduce the possible causes of the decay in the performance to one: the physical setup.
- Duration of the experiment: approximately 10 minutes.
- Method: Cyberglove based. This will allow to compute the errors accurately.
- Position of the probe: Ventral side of the mid-forearm.
- Phases of the experiment:
 1. Train: 6 movements.
 2. Predict: 30 movements.

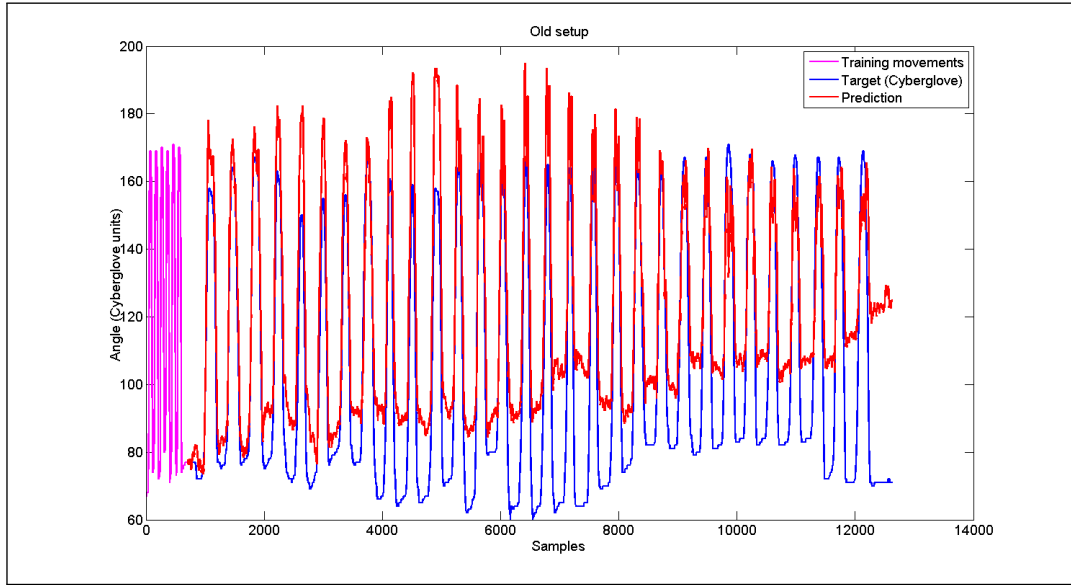
There is no retraining. The target of this experiment is not to evaluate how good the prediction can get but the difference in performance between both setups. A fixed set of repetitions for training and predicting is therefore used. The number of predicting repetitions will be high, for it is in the long run when the differences between the setups are expected to be clear.

- Number of subjects: 1. According to the sensations that both setups transmit when using them and to the common sense (in one of the setups the arm and the probe are completely fixed while on the other the arm is free to slide under the probe) the results are expected to be clear.

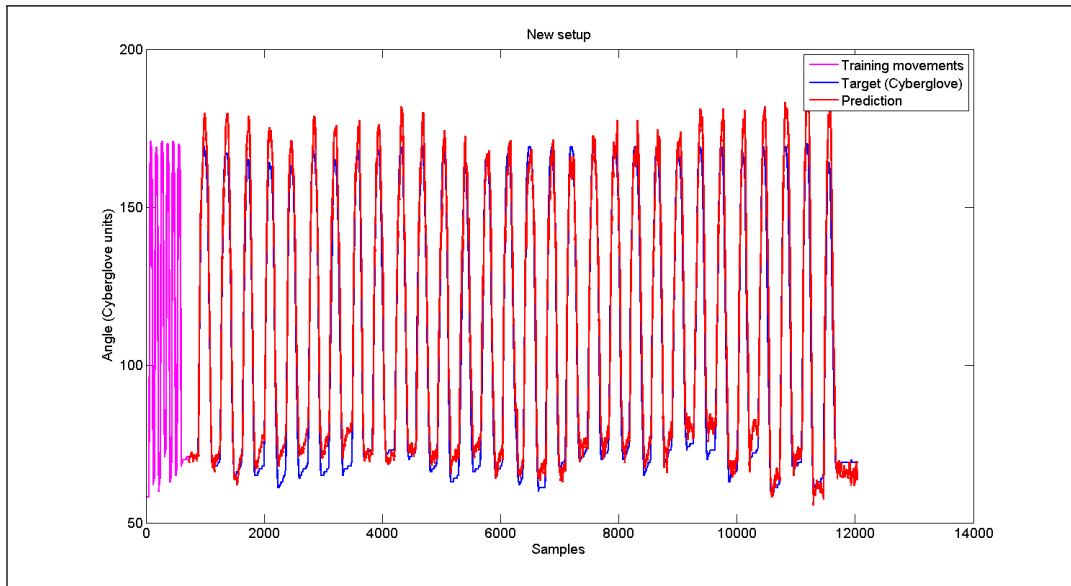
8.1.2 Results

In the first place the evolution of the experiments is shown in figure 8.1. At the beginning of the experiment the 6 movements of training can be observed in pink. Afterwards the prediction phase begins. In blue the target (cyberglobe, real position) is represented while the signal in red is the prediction.

To give a more clear idea of how the quality of the prediction evolves during the experiment the error will be computed for every pack of five prediction movements. This is represented in table 8.1.



(a) Old setup: drill holder



(b) New setup: whole structure

Figure 8.1: Testing of physical setups

8.1.3 Analysis of results

The results are conclusive: the new setup is definitely better. Not only it keeps the quality of the prediction stable over time but also provides a much higher accuracy in the prediction. The performance of the prediction when using the old setup clearly degrades over time. It is really complicated to maintain the arm static under the drill holder and this translates into the bad results, that get worse and worse as the experiment goes on.

Pack of 5 predictions	#1	#2	#3	#4	#5	#6
NRMSE old setup	0.1371	0.1779	0.1995	0.2554	0.2012	0.2636
NRMSE new setup	0.0657	0.0746	0.068	0.0574	0.0761	0.0929

Table 8.1: Evolution of the NRMSE of the two setups during the experiment

Conclusion The new physical setup implemented avoids the relative movements between the arm and the probe and therefore it helps to keep the performance of the prediction constant. This setup will be used in the main experiment.

8.2 Main experiment

8.2.1 Description

The target of the main experiment is to ensure that the system works with different subjects. The US images of the forearm are rather different between subjects; if a good performance of the system were obtained from such different forearm structures that would be a clear sign that the system is ready to be tested on amputees.

With this goal in mind an experiment was conducted on five healthy subjects, all of them males, right-handed and with ages between 22 and 40 years old.

The conditions of the experiment are detailed on table 8.2 and the modes of operation and functions of the 3D hand models are identical to those of table 7.1.

<i>MAIN EXPERIMENT</i>	
Number of subjects	5
Number of phases	Two: Cyberglove-based and stimulus-based
Duration	Over 1 hour
Position of the probe	Mid-forearm, ventral-lateral side
Sequence for each phase	Training: 7 reps/DoF
	Predicting: 6 reps/DoF
	Re-training: 3 reps/DoF ¹
	Testing: 10 reps/DoF

Table 8.2: Conditions of the main experiment

The subjects will test the system in both modalities, Cyberglove-based and stimulus-based, with a duration each of over half an hour. In both modalities the same sequence of finger movements will be used.

¹6 reps/DoF if poor performance was experienced during the first prediction phase

The process begins with a training session of 7 movements for each degree of freedom. It has been empirically learnt that seven repetitions provide a basic working prediction. Following the training session a short prediction round is conducted. Six repetitions in each DoF pretend to give an idea of the quality of the prediction after the first fixed training phase. This short prediction phase is followed by a retraining session, with 3 or 6 movements for each DoF, depending on the quality observed during the prediction. Finally a long testing session of 10 repetitions in each DoF will be performed. The objectives: confirm that the online retraining system works and allows to improve on the fly how the prediction behaves. The duration of the experiments is relatively long to confirm that the system is capable of maintaining a relative good performance over time.

During these experiments the whole physical setup that was tested on the preliminary experiment will be used. The whole experiment setup can be observed in figure 8.2, which displays a picture taken during the training phase. The test subject can be seen following the stimulus given by the hand model with the black background. The hand model with white background is inactive.

On the table lays also the receiver of the Flock of Birds. During the experiment the emitter was placed on the dorsal aspect of the hand. Although the compensation of the wrist pronation is not implemented in this testing version of the system, the relative angle of the wrist with respect the one it had at the beginning of the experiment is displayed on the screen and it helps the subjects to keep the position of the wrist relatively constant.



Figure 8.2: Test subject during the experiment

8.2.2 Results

8.2.2.1 Using Cyberglove

The results of the NRMSE and the CC of the prediction before and after the retraining are presented in tables 8.3 and 8.4 respectively.

Subject		Pinkie	Ring	Middle	Index	Thumb A.	Thumb R.
#1	<i>NRMSE</i>	0.1284	0.2884	0.1217	0.1617	0.1625	0.1751
	<i>CC</i>	0.8506	0.7878	0.8544	0.7615	0.6211	0.7201
#2	<i>NRMSE</i>	0.1075	0.0960	0.0757	0.1318	0.1306	0.1305
	<i>CC</i>	0.9140	0.9547	0.9436	0.9480	0.8007	0.8676
#3	<i>NRMSE</i>	0.0969	0.1284	0.1570	0.1455	0.2356	0.1621
	<i>CC</i>	0.8842	0.7932	0.7693	0.7501	0.5652	0.5172
#4	<i>NRMSE</i>	0.1585	0.1589	0.1584	0.1380	0.2308	0.2819
	<i>CC</i>	0.8264	0.8820	0.8061	0.7869	0.0021	0.3550
#5	<i>NRMSE</i>	0.1805	0.1792	0.1797	0.1348	0.1435	0.1712
	<i>CC</i>	0.3594	0.3704	0.5717	0.7782	0.7342	0.6484

Table 8.3: Prediction results with Cyberglove before retraining

Subject		Pinkie	Ring	Middle	Index	Thumb A.	Thumb R.
#1	<i>NRMSE</i>	0.1276	0.1930	0.0703	0.0823	0.0900	0.0826
	<i>CC</i>	0.8511	0.8973	0.9301	0.9317	0.8412	0.8756
#2	<i>NRMSE</i>	0.0980	0.0716	0.0805	0.0886	0.1005	0.0802
	<i>CC</i>	0.9302	0.9528	0.9215	0.9313	0.7954	0.8972
#3	<i>NRMSE</i>	0.1122	0.1306	0.1409	0.1088	0.1790	0.1786
	<i>CC</i>	0.8448	0.7879	0.7275	0.8416	0.4158	0.4556
#4	<i>NRMSE</i>	0.1350	0.1190	0.1208	0.1827	0.2521	0.1903
	<i>CC</i>	0.7206	0.8577	0.7925	0.7984	0.2455	0.5939
#5	<i>NRMSE</i>	0.1798	0.1236	0.1894	0.1266	0.1528	0.1347
	<i>CC</i>	0.7179	0.8885	0.7740	0.8961	0.6847	0.8040

Table 8.4: Prediction results with Cyberglove after retraining

The comparison of results between tables 8.3 and 8.4 (that is, before and after retraining) can be seen in figures 8.3 and 8.4.

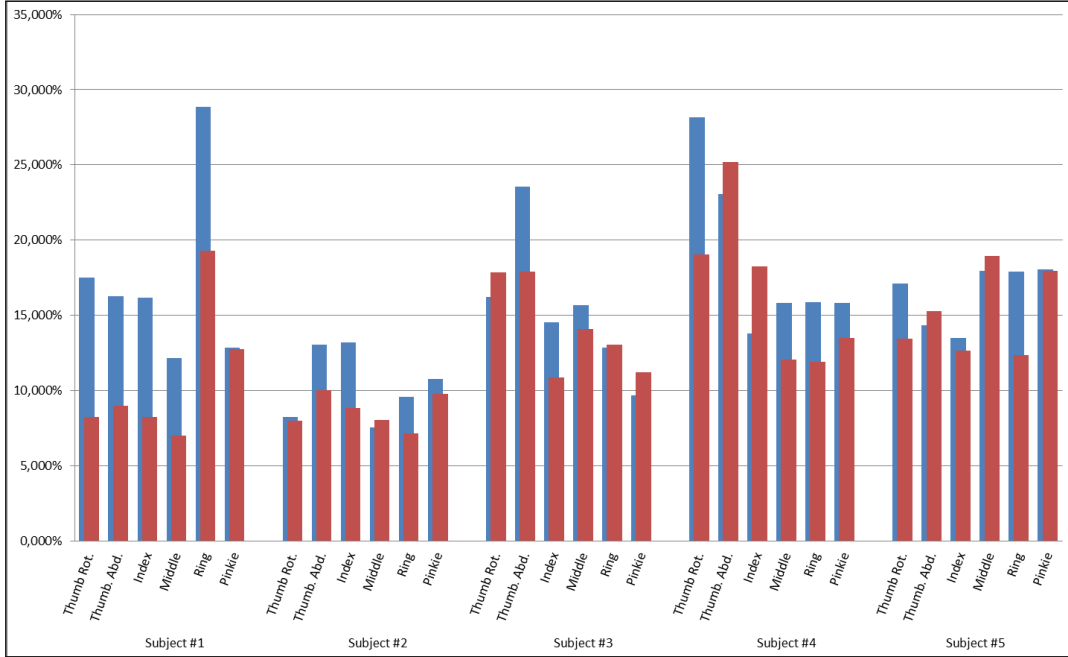


Figure 8.3: Comparison of NRMSE before and after retraining with Cyberglove (blue: before, red: after)

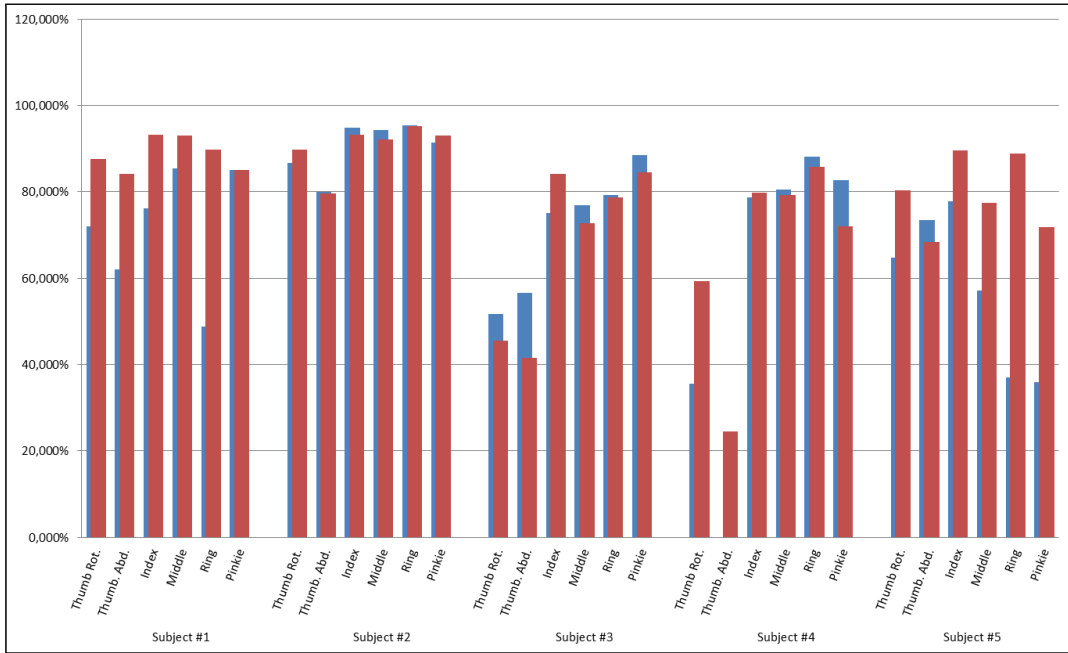


Figure 8.4: Comparison of CC before and after retraining with Cyberglove (blue: before, red: after)

8.2.2.2 Using stimulus

The results of the NRMSE and the CC of the prediction before and after the retraining are presented in tables 8.5 and 8.6 respectively.

Subject		Pinkie	Ring	Middle	Index	Thumb A.	Thumb R.
#1	<i>NRMSE</i>	0.1212	0.1480	0.1352	0.1879	0.1239	0.17
	<i>CC</i>	0.8485	0.8431	0.8705	0.8479	0.7775	0.6282
#2	<i>NRMSE</i>	0.1616	0.1461	0.1770	0.1280	0.0759	0.1105
	<i>CC</i>	0.7245	0.8463	0.8557	0.8973	0.9374	0.8650
#3	<i>NRMSE</i>	0.1862	0.2199	0.1810	0.1289	0.2688	0.37
	<i>CC</i>	0.6843	0.4072	0.6651	0.8205	0.2532	0.5070
#4	<i>NRMSE</i>	0.1197	0.1775	0.1416	0.1164	0.1718	0.1744
	<i>CC</i>	0.9093	0.8432	0.9058	0.8982	0.6097	0.6433
#5	<i>NRMSE</i>	0.1906	0.1428	0.1647	0.1596	0.1302	0.1787
	<i>CC</i>	0.6500	0.8328	0.7922	0.7827	0.8292	0.7731

Table 8.5: Prediction results with stimulus before retraining

Subject		Pinkie	Ring	Middle	Index	Thumb A.	Thumb R.
#1	<i>NRMSE</i>	0.0916	0.0912	0.0833	0.0915	0.1537	0.1581
	<i>CC</i>	0.9230	0.9262	0.9328	0.9187	0.6412	0.6374
#2	<i>NRMSE</i>	0.1226	0.0972	0.1011	0.0665	0.0825	0.0849
	<i>CC</i>	0.8876	0.9388	0.9529	0.9690	0.9327	0.9290
#3	<i>NRMSE</i>	0.0968	0.1191	0.1244	0.0976	0.2473	0.2173
	<i>CC</i>	0.9111	0.8532	0.8626	0.8972	0.0621	0.8086
#4	<i>NRMSE</i>	0.1141	0.1033	0.0951	0.0784	0.1569	0.1629
	<i>CC</i>	0.8825	0.8994	0.9227	0.9391	0.7187	0.6549
#5	<i>NRMSE</i>	0.1872	0.1387	0.1093	0.0898	0.2075	0.2371
	<i>CC</i>	0.6562	0.8288	0.8852	0.9373	0.3462	0.6480

Table 8.6: Prediction results with stimulus after retraining

The data from tables 8.5 and 8.6 can be displayed together to facilitate the comparison. Figure 8.5 and figure 8.6 show the comparison for the NRMSE and the CC, respectively.

As an example of how the experiments were conducted the whole evolution of the index finger of subject #1 during the experiments is shown in figure 8.7.

8.2.3 Analysis of results

The general results are quite satisfactory. The average NRMSE error is typically around the 10%, which for most DoF translates into an error of 10 degrees (value not so easily

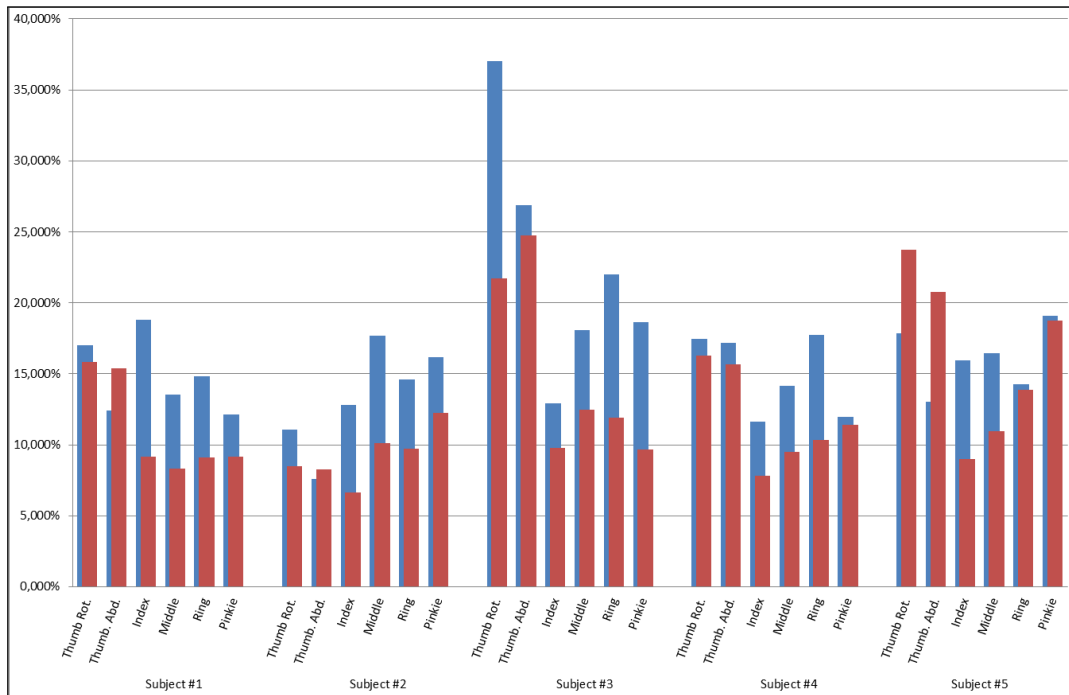


Figure 8.5: Comparison of NRMSE before and after retraining with stimulus (blue: before, red: after)

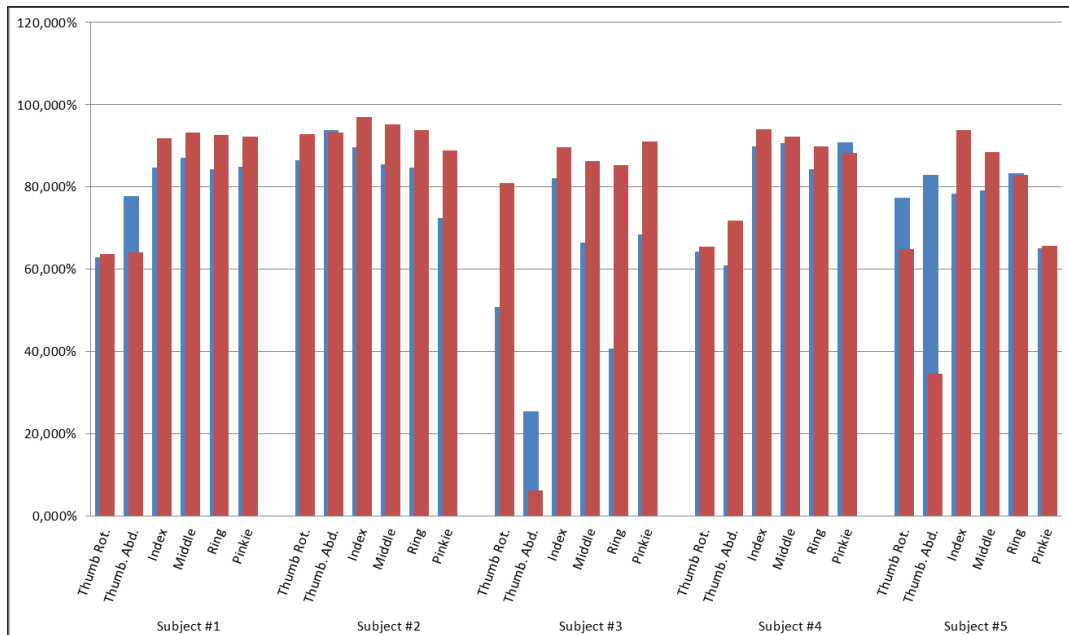
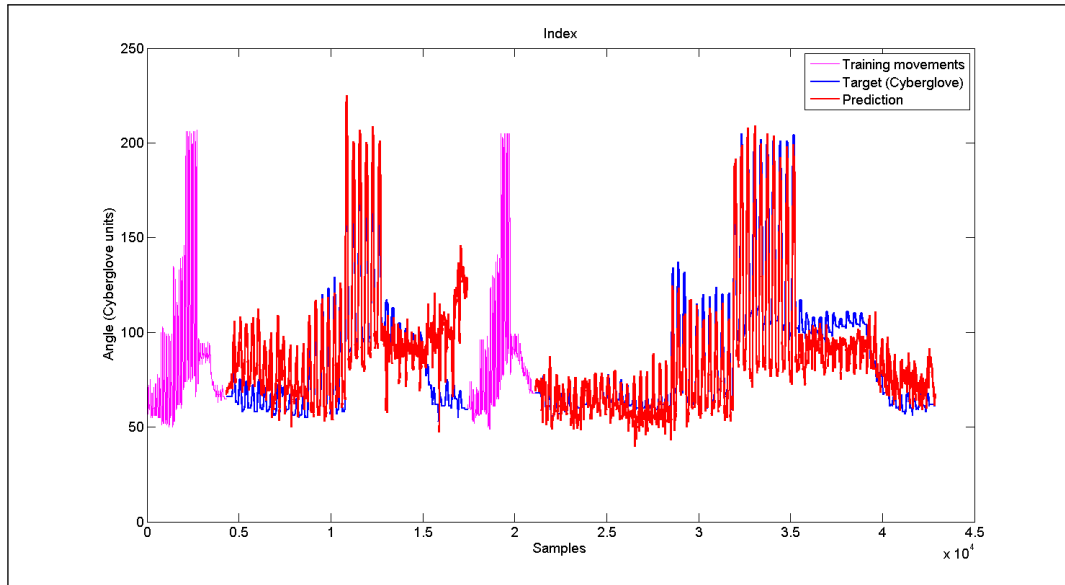
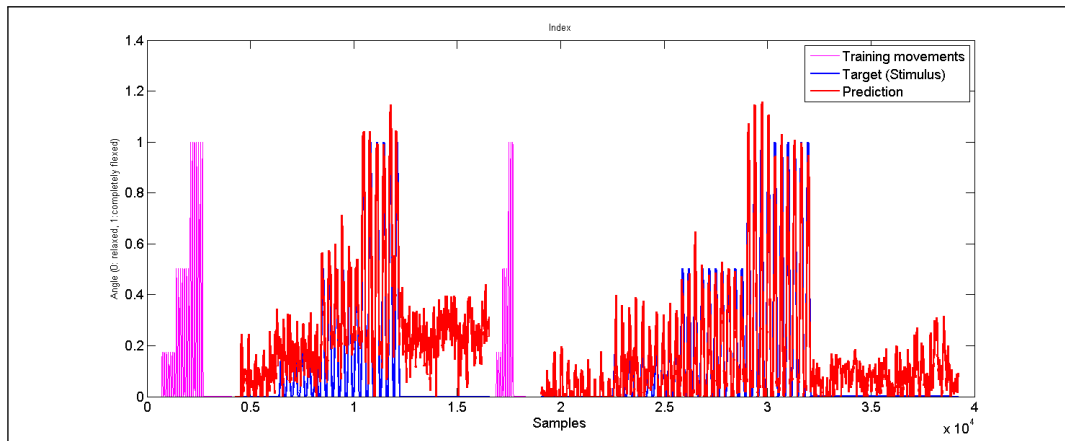


Figure 8.6: Comparison of CC before and after retraining with stimulus (blue: before, red: after)



(a) Evolution of the prediction of the index finger for subject #1 during the experiment with the Cyberglove



(b) Evolution of the prediction of the index finger for subject #1 during the experiment with the stimulus

Figure 8.7: Evolution of the prediction of the index finger for subject #1

noticeable when looking at the hand model on the screen).

A detail must be taken into account when considering the data from the stimulus-based experiment. Since the target data (the stimulus) and the movements of the patients are not 100% synchronized, there is a delay that magnifies the real values of the error in the prediction. However, the results obtained are still rather good. This confirms the good sensations perceived during the experiment. The subjects were quite satisfied and surprised by the good behavior of the system using the stimulus.

It has been a 100% proved, that by means of a short retraining session the performance of the system can be boosted. Both using the Cyberglove or the stimulus, most of the errors computed had been reduced after the retraining session. The number of retraining series was already fixed beforehand. In a real experiment the retraining would continue until the patient is satisfied with the quality of the prediction.

For most of the test objects it was not possible to locate a position on the forearm to place the transducer of the ultrasound system in which the six degrees of freedom were clearly distinguishable. When the two DoF associated to the thumb where into focus the rest of the DoF were not, and vice versa. Most of the subjects present indeed the bigger errors in the thumb related degrees of freedom.

Subjects #1 and #2 had already tried the system before the experiment was conducted. These two subjects present on average smaller errors in the prediction than the others. From this it is possible to conclude that patients learn from experience and that the more they use the system the better prediction quality they will obtain. As a final product, a training period would be necessary before the patients could benefit from the true capabilities of the system.

Figure 8.7 confirms that the accuracy of the prediction improves with the retraining. Another aspect to consider from this figure is that the performance of the system remains relatively stable, as a consequence of the improved physical setup and of the effort of the test subjects trying to keep the angle of the wrist as stable as possible, guided by the measure of the Flock of Birds presented on the GUI.

9

Conclusions and future work

Previous studies had shown that ultrasound image features of the forearm are linearly related to finger positions. A system had been implemented proving that it was possible to predict online the hand configuration from a stream of ultrasound images of the forearm.

The general objective of this thesis was to take that system a step further, improving the accuracy of the prediction and the stability of the system on the long run.

The new online training system, with its ability to change dynamically from the training phase to the prediction phase and vice versa, allows a *fine training* for each degree of freedom, thus increasing the accuracy. The new training system affects also the stability of the system. In case of any external perturbation during the experiment that could change the conditions of the system, simply switching to the training mode and adding more data to the affected degrees of freedom would get the system back to the optimal point, whereas previous iterations of the project would be forced to start the experiment from the beginning.

The results obtained from the main experiment show the efficacy of this approach. After a fixed number of training movements a short prediction round was conducted to check the

quality of the prediction at that point. Afterwards, a fixed round of retraining movements was executed followed by a long prediction phase. For almost all patients, there is a clear improvement of the prediction from the first prediction part of the experiment to the second.

With the new physical setup the probe is completely fixed to the arm during the whole experiment, thus avoiding changes in the characteristics of the images and by extension in the quality of the prediction. The preliminary experiment with the old setup proves that the quality of the prediction holds with the new probe holder, whereas with the old one, which consisted only on a drill holder, the quality of the prediction degrades.

Thanks to the graphical user interface the system is very intuitive and easy to use. Calibrating the Cyberglove at the beginning of the experiment, switching back and forth from prediction to training, choosing which data to save to the disk or simply watching a representation of the target features change in real-time superimposed over the ultrasound images are some of the perks that this interface offers.

The two main problems encountered have been:

- High impact of the changes in the angle of the wrist on the quality of the prediction. The slightest pronation of the wrist during the experiments produces a very noticeable change in the ultrasound images. It is not physically possible to fix the wrist to the structure in a way that these tiny movements were no longer doable. Therefore, a software solution based on a magnetic tracker called Flock of Birds is proposed. The grid of circles in charge of extracting the numeric features out of the ultrasound frames shifts in a proportional manner to the angle of the wrist, tracking this way the visual features. It is estimated that this system could reduce by 50% the error induced by the wrist pronation.
- Impossibility for the two degrees of freedom of the thumb to be clearly captured together with the movements of the other digits. As stated in section 4.2 the muscles in charge of rotating and abducting the thumb are different than those in charge of flexing the rest of the fingers. It has not been possible with the test subjects to find a spot for the probe where the 6 degrees of freedom could offer clear changes in the ultrasound images. If the place is chosen in a way that the images show clear changes when flexing the pinkie, ring, middle and index, then the changes in the images when rotating and abducting the thumb will be subtle, and the errors high. This fact is clearly observable by examining the results obtained from the main experiment.

The system will need to overcome these problems to achieve the necessary precision required to control prosthetic hands. However, based not only in the numbers obtained from the main experiment but on the sensations the subjects expressed while performing them, the system could already be an option to deal with patients affected by phantom limb pain

or neuropathic pain in the upper limbs. Especially when using the stimulus-based version of the system the results were very satisfactory, although this does not translate into low errors due to the delays of the target and guessed signals.

Improvements over previous work The advancements that this work provides over previous iterations of the project are summarized in the list below:

- Implementation of an *online training system* that facilitates each degree of freedom to be trained individually and as much as necessary until the desired quality of prediction is achieved. The changes from training to predicting and vice versa are dynamic, instantaneous and can happen at any time during the experiment. This is a big difference compared to the old versions in which the system was trained at the beginning of the experiment and there was no option to retrain. A change in the conditions of the experiment, e.g. the patients moves, would mean that the experiment had to be restarted from the beginning.
- Development of a Graphical User Interface that is the natural complement of the online training system, allowing the user to control the course of the experiment.
- The code of the new system has been written from scratch in C#. The new code is clear, legible and well organized using different files, each associated to a different piece of hardware or function of the system. The way the data from the different devices is synchronized has been simplified and adapted to the online approach.
- Realistic data on the accuracy and reliability of the system is provided. The analysis is based exclusively on data obtained from the prediction during the experiments. In the past, the whole data of the experiment was saved to the disk and, by means of machine learning techniques, computed to analyze the feasibility of the project.
- Improvement of the physical setup used to carry out the experiments. The preliminary experiment has shown how weak and unreliable the previous setup was. The new setup succeeds at getting the probe fixed to the arm during the whole extension of the experiment, yielding therefore much better and comparable results.
- Analysis of the system during long-time experiments. The new physical setup has stopped the negative influence of the movements of the probe with respect of the arm. However a new problem has arisen. During long time experiments subjects tend to pronate the wrist in a way that no physical setup can avoid, with translates into a modification of the ultrasound images. A new theoretical approach is discussed in order to tackle this problem.

Future work This project has been developed over a period of five months. During this time a number of improvements over the previous system have been achieved and new

ideas have arisen and should be looked into in the next iterations of the project.

Several interesting directions for future work that would help expand and strengthen the results are the following:

- Test the system on amputees. Initial contacts have already been made and the arrival of patients should not delay much longer. From past experiences it is known that amputees can provide completely different ultrasound images with the movement of each degree of freedom (although also with the difficulty to get different images for the six degrees of freedom). Therefore, the same degree of performance as the one obtained with healthy patients in this thesis is expected.
- Implement a system capable of deciding when to stop the training phase and begin predicting. The thresholds of acceptable error would be the only necessary input. The system could integrate short prediction rounds within the training phase and evaluate the error upon them. For each DoF if the error is below the threshold then there is no need to train that specific DoF further.
- Expand the number of DoF that the system can handle. The integration of the PIP and DIP joint movements would yield a completely realistic simulation of how the fingers move. The Cyberglove has the necessary sensors and the US images display clear differences when performing these additional movements, consequently making this step achievable.
- If new DoF are incorporated into the system the complexity of it will obviously rise. Exploring more advanced machine learning techniques, like Support Vector Machines, would then be very recommended.
- Integrate the Flock of Birds wrist compensation into the system. The changes in the ultrasound images when even the slightest modification of the wrist angle occurs are, without any doubt, the main cause responsible of the decay in the performance during the predictions. Tracking the angle and compensating the images in a proportional way would yield the definitive robust system. However, the changes in the muscles and tendons in the wrist during the finger movements can cause instability in the magnetic tracker and introduce noise in the system. Machine vision approaches could be considered to track the angle instead.
- Upgrading the hardware of the system is something that probably figures in every thesis. Yet in this case an improvement in the way the ultrasound data is fed into the system would certainly have a positive impact on the performance. Either by having an ultrasound system capable of streaming the images directly to the computer or by upgrading the VGA framegrabber to one capable of synchronizing with the ultrasound unit would avoid the teared-frames problem and shorten the processing times. Moreover, with the available transducer of the ultrasound system it is not

possible to capture clearly the six targeted movements. A search for a new transducer or, if need be, an additional US system is suggested.

Final comments The period of five months over which this thesis was developed has been a time of hard work, full of ups and downs, as the system was slowly progressing. I have had an insight view of the research world at one of the most advanced technological institutes of the world. Research is very hard work, time-consuming and a field in which work does not necessarily translate into positive results. Nothing of that matters however, when everything falls into place and you get to push the limits of science a bit further. One of the personal conclusions I came to during this time is that there is nothing more satisfactory than to work on something that will eventually help other people and make their lives better.

To summarize, this work has had a tremendous positive impact on myself, both personal and professionally, and hopefully someday patients affected by phantom limb pain or neuropathic pain will be able to alleviate their pain with the help of the system presented on this thesis.

References

- [1] Image taken from <http://endthepainproject.org>, 2012.
- [2] Claudio Castellini and Georg Passig. Ultrasound image features of the wrist are linearly related to finger positions. In *Intelligent Robots and Systems (IROS), 2011 IEEE/RSJ International Conference on*, pages 2108–2114, 2011.
- [3] G. A. W. Bruyn and W.A. Schmidt. *Guide to Musculoskeletal Ultrasound for the Rheumatologist*. Bohn Stafleu van Loghum, 2005.
- [4] SensorHand Speed (Ottobock) <http://www.ottobock.com>, 2012.
- [5] i-limb ultra (Touch Bionics) <http://www.touchbionics.com/products/active-prostheses/i-limb-ultra>, 2012.
- [6] V. Florimond. *Basics of Surface Electromyography applied to Physical Rehabilitation and Biomechanics*. Thought Technology Ltd, 2010.
- [7] Toshiharu Kishi and Wenwei Yu. Finger motion recognition by skin surface vibration patterns. *International Journal of Bioelectromagnetism*, 9(2):57–58, 2007.
- [8] Claudio Castellini and Patrick van der Smagt. Surface emg in advanced hand prosthetics. *Biological Cybernetics*, 100(1):35–47, 2008.
- [9] Ryan J. Smith, Francesco Tenore, David Huberdeau, Ralph Etienne-Cummings, and Nitish V. Thakor. Continuous decoding of finger position from surface emg signals for the control of powered prostheses. In *30th Annual International IEEE EMBS Conference*, pages 197–200, 2008.
- [10] Claudio Castellini, Georg Passig, and Emanuel Zarka. Using ultrasound images of the forearm to predict finger positions. 2012.
- [11] Jun Shi, Qian Chang, and Yong-Ping Zheng. Feasibility of controlling prosthetic hand using sonomyography signal in real time: Preliminary study. *Journal of Rehabilitation Research & Development*, 47(2):87–98, 2010.
- [12] Xin Chen, Yong-Ping Zheng, Jing-Yi Guo, and Jun Shiy. Sonomyography (smg)

- control for powered prosthetic hand: a study with normal subjects. *Ultrasound in Medicine and Biology*, 36(7):1076–1088, 2010.
- [13] Image taken from <http://www.touchbionics.com>, 2012.
- [14] Emanuel Richard Zarka. Prediction of finger movements using ultrasound images. Master’s thesis, University of Applied Sciences Technikum Wien, 2011.
- [15] Samer N. Narouze. *Atlas of Ultrasound-Guided Procedures in Interventional Pain Management*. Springer, 2010.
- [16] Steven M. Penny, Traci B. Fox, and Cathy Herring Godwin. *Sonographic Principles & Instrumentation*. Lippincott Williams & Wilkins, 2011.
- [17] Barry C. Simon and Eric R. Snoey. *Ultrasound in Emergency and Ambulatory Medicine*. Elsevier Health Sciences, 1997.
- [18] Michael McKinley and Valerie O’Loughlin. *Human Anatomy*. McGraw-Hill Science/Engineering/Math, 2005.
- [19] <http://en.wikipedia.org/wiki/Forearm>, 2012.
- [20] Johannes Sobotta. *Atlas of Human Anatomy Volume 1: Head, Neck, Upper Limb*. Churchill Livingstone, 2006.
- [21] Mike Bradley and Paul O’Donnell. *Atlas of musculoskeletal ultrasound anatomy*. Cambridge University Press, 2002.
- [22] R. T. Floyd. *Manual of Structural Kinesiology*. McGraw-Hill Humanities/Social Sciences/Languages, 2011.
- [23] Herta Flor. Phantom-limb pain: characteristics, causes and treatment. *The Lancet Neurology*, 1(3):182–189, 2002.
- [24] Martin M. Malawer, Paul H. Sugarbaker, and Lee-Ann Rhodes. *Musculoskeletal Cancer Surgery: Treatment of Sarcomas and Allied Diseases*. Springer, 2001.
- [25] V. S. Ramachandran and D. Rogers-Ramachandran. Synaesthesia in phantom limbs induced with mirrors. *Proceedings of The Royal Society B: Biological Sciences*, 263(1369):377–386, 1996.
- [26] <http://www.coursera.org/course/ml>, 2012.
- [27] Christopher M. Bishop. *Pattern recognition and machine learning*. Springer, 2006.
- [28] Arjan Gijsberts. *Incremental learning for robotics with constant update complexity*. PhD thesis, University of Genoa, 2011.
- [29] National Instruments. *NI Vision: IMAQ vision concepts manual*. 2005.

-
- [30] MVTec Software GmbH. *HALCON/HDevelop reference manual*, 2010.
 - [31] J.L.Barron and N.A.Thacker. *Computing 2D and 3D Optical Flow*. TINA-Vision, 2005.
 - [32] GE Healthcare. *LOLIGe Basic Service Manual*, 2006.
 - [33] <http://www.epiphan.com/products/frame-grabbers/vga2ethernet/>, 2012.
 - [34] <http://www.ascension-tech.com/realtime/rtflockofbirds.php>, 2012.
 - [35] <http://www.mvtec.com/halcon/>, 2012.
 - [36] <http://www.alglib.net/>, 2012.